Memory trace interference impairs recall in a mouse model of Alzheimer's disease

Stefanie Poll[1*], Manuel Mittag[1], Fabrizio Musacchio[1], Lena C. Justus[1], Eleonora Ambrad Giovannetti[1], Julia Steffen[1], Jens Wagner[1], Lioba Dammer[2], Susanne Schoch[2], Boris Schmidt[3], Walker S. Jackson[4], Dan Ehninger[5] and Martin Fuhrmann[1*]

[1]Neuroimmunology and Imaging Group, German Center for Neurodegenerative Diseases (DZNE), Bonn, 53127, Germany.

[2]Institute of Neuropathology, University of Bonn, 53127, Germany

[3]Clemens-Schöpf-Institute, Technical University of Darmstadt, 64289, Germany

[4]Selective Vulnerability of Neurodegenerative Diseases, German Center for Neurodegenerative Diseases (DZNE), Bonn, 53127, Germany

[5]Molecular and Cellular Cognition Group, German Center for Neurodegenerative Diseases (DZNE), Bonn, 53127, Germany

[*]Corresponding Authors:

Dr. Martin Fuhrmann (lead contact) and Dr. Stefanie Poll

Center for Neurodegenerative Diseases (DZNE), Bonn

Sigmund-Freud-Str. 27

53127 Bonn

Germany

E-mail: martin.fuhrmann@dzne.de; stefanie.poll@dzne.de

Abstract

In Alzheimer's disease (AD), hippocampus-dependent memories underlie an extensive decline. The neuronal ensemble encoding a memory, termed engram, is partly recapitulated during memory recall. Artificial activation of an engram can restore memory in a mouse model of early AD, but its fate and the factors that render the engram nonfunctional are yet to be revealed. Here we used repeated two-photon *in vivo* imaging in fosGFP transgenic mice that performed a hippocampus-dependent memory task. We found that the partial reactivation of the CA1 engram during recall is preserved under AD-like conditions. However, we identified a novelty-like ensemble that interfered with the engram and thus compromised recall. Mimicking a novelty-like ensemble in healthy mice was sufficient to affect memory recall. In turn, reducing the novelty-like signal rescued the recall impairment under AD-like conditions. These findings suggest a novel mechanistic process that contributes to the deterioration of memories in AD.

Introduction

Memories are the results of our past experiences and crucial for our everyday life. The presence of neural correlates underlying and serving memory formation during learning was hypothesized already almost a century ago[1]. These neuronal correlates - termed engram or memory trace[2] - are partly reactivated during memory recall[3,4] .Memory traces are identified[5] with the help of immediate early gene (IEG) expression that serves as a correlate of neuronal activity[6-8] and activity-dependent plasticity[9]. The manipulation of memory traces has led to valuable insights in the relevance of these neuronal ensembles for memories and associated behavior in various brain regions[2].

In Alzheimer's disease (AD), the most common form of dementia[10,11], declarative memories are subject to decline[12,13]. This symptom is associated with severe pathophysiological changes in the hippocampal CA1 region in AD[14]. CA1 serves as the main output region of the hippocampus and is crucial for contextual memory formation and retrieval[15]. It is furthermore proposed to be involved in novelty detection in rodents and humans, due to its ability to act as a comparator between past and present experiences[16-18]. In mouse models with AD-like pathology, CA1 neurons show aberrant activity in close proximity to amyloid-β plaques (Aβ plaques)[19,20], a pathological hallmark of the disease. In addition, aging, a major risk factor of AD, leads to altered contextual representations in CA1[21]. The artificial silencing of a CA1 engram impairs memory recall[22] and results in the emergence of an alternative engram that presumably neutralized a learned association[23]. The artificial reactivation of a contextual engram was sufficient to induce the recall of the memory[24], even under amnesic[25] and AD-like conditions[26]. However, the actual fate of the hippocampal CA1 engram in the context of AD-related memory loss and the underlying mechanisms are still unknown.

Here we used repetitive hippocampal two-photon *in vivo* imaging in IEG reporter mice during hippocampus-dependent learning and memory. We revealed an intact contextual

63 engram under AD-like conditions in hippocampal CA1 and identified an additional
64 ensemble interfering with memory recall. Artificial activation of an interfering ensemble
65 impaired memory in healthy mice, whereas suppression of the interfering ensemble
66 rescued memory deficits under AD-like conditions.
67
68 **Results**
69 **FosGFP expression revealed two sub-populations of CA1 pyramidal neurons**
70 To investigate cellular correlates of memory under healthy and AD-like conditions
71 through the IEG *Fos*, we crossbred fosGFP[27] mice with the APPswe/PSEN1dE9[28]
72 (APP/PS1) mouse model of AD. To monitor fosGFP expression changes in CA1
73 pyramidal neurons of the dorsal hippocampus upon memory acquisition and recall, we
74 implanted a chronic cranial window above this region and carried out two-photon *in vivo*
75 imaging as previously described[29] (Fig. 1a). We assessed fosGFP expression in the
76 same population of neurons daily, first without behavioral stimulus (BL, baseline fosGFP
77 expression) and then upon contextual fear conditioning (cFC) and subsequent memory
78 recall (test), a hippocampus-dependent learning and memory task (A-A and A-B,
79 conditioning in A and test in either A or B) (Fig. 1b). Neurons that showed an increase in
80 fosGFP expression were associated with higher neuronal activity during initial novel
81 context exposure (~ 90 min before), compared to neurons that showed a decrease or no
82 change in fosGFP expression (Extended Data Fig. 1). This is in line with a recent study
83 showing that fosGFP expression is correlated with learning-related activity changes[30].
84 Only ~1% of all fosGFP-positive (fosGFP$^+$) neurons were inhibitory (GAD67$^+$) suggesting
85 that the majority of fosGFP$^+$ neurons within the CA1 pyramidal layer were excitatory
86 (Fig. 1c-e). Even though we probably slightly overestimated endogenous
87 proto-oncogene c-Fos (c-Fos) by measuring fosGFP expression - possibly due to the
88 longer half-life of GFP compared to c-Fos - we rarely detected endogenous c-Fos

89 expressing cells that were fosGFP-negative (Extended Data Fig. 2a-d). This indicates
90 that fosGFP represents the majority of endogenous c-Fos expression. In fosGFP-
91 APP/PS1 mice the density of fosGFP$^+$ neurons was comparable to healthy littermates,
92 whereas the fluorescence intensity was altered in proximity to Aβ plaques (Extended
93 Data Fig. 2e-m). This is in line with previous work showing aberrant expression levels of
94 IEGs in different mouse models of AD[31,32] as well as in human AD brains[33,34]. However,
95 daily fosGFP expression changes under baseline conditions in fosGFP-APP/PS1 mice
96 were comparable with those of healthy littermates, indicating no disturbance of the CA1
97 neuronal network on this level (Fig. 1f-i). A large fraction (~60%) of fosGFP$^+$ neurons
98 maintained their expression from one day to the other (CON = continuous expression),
99 whereas the remaining fraction switched expression on a daily basis (ON = expression
100 switched on, OFF = expression switched off) (Fig. 1f-h). Both populations, CON and
101 ON/OFF, remained constant during the baseline period, underscoring the stability of the
102 hippocampal network in both genotypes (Fig. 1g,h). Our data suggest the existence of
103 two neuronal sub-populations in CA1: these could either represent stable (CON) and
104 varying (ON, OFF) contextual or spatial aspects of the environment[35], or incorporate
105 temporal information that is coded by CA1 over different scales, ranging from seconds
106 and minutes to days[36].
107
108 **Learning-induced fosGFP expression is intact in CA1 of fosGFP-APP/PS1 mice**
109 In accordance with previous studies[37,38] APP/PS1 transgenic mice displayed significantly
110 reduced contextual fear memory (Fig. 1j), associated with impaired memory acquisition
111 on the behavioral level (Extended Data Fig. 3a,b). We excluded differences in
112 exploratory behavior between fosGFP and fosGFP-APP/PS1 mice by measuring the
113 travelled distance in context A before conditioning (pre-shock) (Fig. 1k and Extended

Data Fig.3b). After conditioning in context A, exposure of both fosGFP and fosGFP-APP/PS1 mice to a novel, but similar context (context B) led to low freezing behavior, validating the context specificity of memory recall (Fig. 1l). We hypothesized that the impairment in memory acquisition and recall of fosGFP-APP/PS1 mice was reflected on the neuronal network level by altered fosGFP expression. In contradiction to our hypothesis we found a twofold increase of ON neurons upon memory acquisition in both, fosGFP and fosGFP-APP/PS1 mice (Fig. 1m,n). This indicates that learning-induced fosGFP expression is intact in CA1 under AD-like conditions. Similarly, endogenous c-Fos expression in CA1 did not reflect the short-term memory deficit of APP/PS1 mice (Extended Data Fig. 3c-f). On the day after memory acquisition, we detected an increase of OFF neurons in fosGFP and fosGFP-APP/PS1 mice, suggesting that the network activity returned to baseline levels (Fig. 1m,n). Upon memory recall in context A, the number of ON neurons was not altered compared to the day before conditioning (d0-1) in fosGFP mice (Fig. 1m and Supplementary Table 1). This finding is in accordance with previous results showing that c-Fos expression in CA1 is mainly elevated in response to exploration of novel rather than familiar environments or to exposure to aversive stimuli alone[39]. Indeed, exposing fosGFP and fosGFP-APP/PS1 mice to a novel context B on the test day led to a twofold increase of ON neurons, comparable to the increase after conditioning (Fig. 1o,p). Interestingly, re-exposing fosGFP-APP/PS1 mice to the conditioned and thus familiar context A resulted in a similar increase of their ON population (Fig. 1n), showing a tendency in the inter-group comparison (Extended Data Fig. 4). The total number of ON neurons was increased in mice exposed to a novel context B and fosGFP-APP/PS1 mice tested in context A (Fig. 1q). The number of CON neurons remained stable over time in all experimental groups. We further tested whether the population of ON cells detected upon cFC represents a memory trace. Indeed, optogenetic activation of this CA1 ensemble that

expressed c-Fos upon learning was sufficient to artificially induce freezing in APP/PS1 mice to the same extent as in wild-type mice (Extended Data Fig. 5). This is in line with, and further extends, previous findings showing that CA1 activity is necessary[15,22] and sufficient[25] for recent and remote memory recall. Moreover, this validates that CA1 neurons expressing c-Fos upon learning comprise a neuronal ensemble relevant for memory recall. In addition, our *in vivo* fosGFP data revealed an intact c-Fos expression increase in CA1 upon learning in APP/PS1 mice.

Sparse CA1 engram occurs independent of memory

We then sought to describe the fate of the memory-relevant ensemble during "natural" recall and investigate the relevance of individual neurons' activity history. For this, we calculated the relative frequency of all possible fosGFP expression patterns based on the data in Fig. 1 (Fig. 2a-f). The expression of fosGFP in neurons that started to express fosGFP upon cFC (ON) did not persist on the day following behavioral testing for the majority of this population, and was also not induced by memory recall (Fig. 2g). Only a fifth of the initially activated neurons were reactivated during recall. Only a tenth of neurons that had been fosGFP-positive the day before conditioning (CON) were reactivated (Fig. 2h). Counterintuitively, the reactivated ensembles that expressed fosGFP upon learning was of similar size under healthy and under AD-like conditions, comprising around 15% of the initially active ensemble (Fig. 2i). Moreover, the relative frequency of reactivated neurons (pattern C and I) increased in all four experimental groups (Fig. 2j), indicating that potential engram cells were present regardless of memory performance in the three experimental groups that exhibited decreased freezing (G_2, fosGFP-APP/PS1 A-A; G_3, fosGFP A-B and G_4, fosGFP-APP/PS1 A-B) as well as in mice with intact memory recall (G_1, fosGFP A-A) (Fig. 1j,l, Fig. 2j). Hence, we hypothesized that memory deficits in fosGFP-APP/PS1 mice might be reflected on the

network level by neuronal ensembles interfering with the memory trace during recall. Therefore, we analyzed the fosGFP expression history of neurons that were fosGFP$^+$ upon recall and thus constituted the recall network (RN) (Fig. 3a). Among the possible fosGFP expression patterns, three patterns (C, F, I) displayed a clear change in the relative frequency between baseline (BL) and the learning and memory period (A-A/B) (Fig. 3a,b). Pattern C and I, representing reactivated neurons, increased in relative frequency to a similar extent in all four experimental groups confirming our previous finding that potential engram cells are present independent of memory (Fig. 3c). Surprisingly, pattern F, comprising neurons with first-time fosGFP expression upon memory recall, was only increased in mice with impaired memory (G_2, fosGFP-APP/PS1 A-A) and those exposed to a novel context (G_3, fosGFP A-B and G_4, fosGFP-APP/PS1 A-B), compared to those successfully recalling the context (G_1, FosGFP A-A) (Fig. 3d). Since these neurons potentially encoded novel context information (test in context B), we termed these neurons novelty-like cells. Next, we determined the ratio of engram cells to novelty-like cells for each group in order to assess engram cell frequency relative to novelty-like cell frequency. In accordance with the behavioral performance of the mice, this ratio was significantly increased only in G_1 (fosGFP A-A), but not in G_2, G_3 and G_4 (Fig. 3e). Comparing the complete recall network of the four experimental groups by calculating a correlation coefficient matrix of their relative pattern frequency changes revealed that the neuronal network composition of fosGFP-APP/PS1 A-A mice (G_2) displayed a configuration similar to fosGFP mice exposed to a novel context B (G_3) (Fig. 3f and Supplementary Table 2). Our finding suggests that fosGFP-APP/PS1 mice perceive the familiar context A as novel, resulting in the interference of novelty-like ensembles with the otherwise intact engram and thus impeding memory recall (Fig. 3g).

Reducing novelty-like activity ameliorates memory recall in APP/PS1 mice

To test whether novelty-like ensemble activity in CA1 was sufficient to affect memory recall, we induced activity with DREADDS (designer receptors exclusively activated by designer drugs) in excitatory neurons. The artificial activation of glutamatergic neurons in CA1 during memory recall decreased freezing to the conditioned context (Extended Data Fig. 6). Instead of artificially activating a large subset of CA1 neurons, we next mimicked a novelty-like cell ensemble by activating only neurons that encoded a novel context (context B). Indeed, artificial activation of neurons encoding a novel context B decreased freezing in the conditioned context A (Fig. 4a-f and Extended Data Fig. 7). Moreover, silencing neurons encoding a novel context B (Extended Data Fig. 8), to reduce novelty-like cell activity during recall, rescued memory deficits of APP/PS1 mice (Fig. 4g-k), excluding any unspecific effects of CNO (clozapine-N-oxide) or tagging alone (Extended Data Fig. 9 and Extended Data Fig. 10). In summary, our results indicate that novelty-like activity in CA1 interferes with memory recall. Accordingly, the reduction of novelty-like activity restored memory in APP/PS1 mice.

Discussion

Our analysis of fosGFP expression dynamics in hippocampal CA1 revealed two sub-populations of pyramidal neurons - one maintaining fosGFP expression on a daily basis and another switching it on and off. This suggests a different role of both populations in information processing, in line with the fact that CA1 is increasingly recognized as heterogeneous population of neurons[40].

According to this, we found the potential contextual engram to be part of both sub-populations by constituting 15% of the population active during learning. Our finding of a sparse and transient engram cell ensemble supports the hypothesis that memory traces in hippocampal CA1 are rapidly refined, thereby increasing the efficiency of information processing[2,41,42]. Although we did not investigate reactivation during remote memory

218 recall, we suspect the engram to be sparser and hardly visible on the level of CA1
219 fosGFP expression. This hypothesis is based on the memory index theory, which
220 postulates that the hippocampus serves as an indexing system for complex
221 representations of context manifested in cortical networks[35].
222 In our study, impairment of hippocampus-dependent memory under AD-like conditions
223 was associated with the presence of novelty-like cells in the recall network, presumably
224 interfering with engram cells, rather than with the absence of the memory engram.
225 Although we found the memory trace to be intact on the level of fosGFP expression, we
226 cannot exclude impairments beyond the reporters' temporal and spatial resolution, for
227 example in coordinated firing of CA1 pyramidal neurons or downstream connectivity.
228 Accordingly, novelty-like cells found under AD-like conditions might resemble an
229 alternative engram that was observed during optogenetic inhibition of the retrieved
230 engram in CA1[23]. Here, the alternative engram could act as a competing memory trace.
231 It was shown before that the artificial activation of a competing memory trace was
232 sufficient to interfere with recall of the conditioned context[43]. In this study[43] the memory
233 trace was artificially activated across all brain regions, in contrast to our CA1-specific
234 study.
235 By mimicking novelty-like activity, we cannot exclude an associated "safety" or "non-
236 aversive" component within the artificially activated ensemble that reduced freezing.
237 However, our data argue against this possibility as memory interference worked equally
238 well with a randomly activated set of neurons without any associated context or valence
239 (Extended Data Fig. 6). This is in line with previous findings that even a slight stimulation
240 of the hippocampal formation was sufficient to impair spatial memory[44]. We thus
241 conclude that the novelty-like ensemble and not the associated valence is the
242 dominating factor that interferes with recall.
243 Reducing potential novelty-like ensemble activity had a beneficial effect on memory

244 under AD-like conditions. A different interpretation of Fig.4g-k would be that exposure to
245 context A elicited both, recall of the safety-associated context B and fear-associated
246 context A and thus, silencing of context B ensembles resulted in an increased freezing
247 response due to the dominating fear recall. However, our freezing data in Fig. 1l as well
248 as the cellular data in Fig. 3f indicate that APP/PS1 mice discriminate context A and
249 context B very well, despite their impairment in recalling context A. Therefore, we
250 conclude that inhibition of the context B ensemble decreases the possibility of novelty-
251 like activity and thereby increases engram contrast. Vice versa, we propose that novelty-
252 like neural activity in the recall network interferes with successful recall on the behavioral
253 level, presumably by perturbing information flow. This mechanism might even apply for
254 fosGFP mice exposed to the novel context B (G_3) that as well show context A engram
255 cells during recall in context B. The presence of a novelty-like ensemble in a familiar
256 environment would hence indicate a defect in CA1's function as a comparator between
257 past and present contextual experiences under AD-like conditions. Our data suggest that
258 CA1 wrongly detect a mismatch between the perceived context during recall and the
259 memory of the past experience during conditioning, mistakenly categorizing a known
260 context as novel (Fig. 2f). A similar mis-classification phenotype was shown in CA1 of
261 aged mice[21]. Here, two visits of the same environment resulted in less similar CA1
262 representations compared to young mice. Hence the question is what mechanism
263 underlies the mis-classification phenotype? Previous studies showed that the concerted
264 arrival of precisely timed inputs from CA3 and entorhinal cortex (EC) at different dendritic
265 compartments of CA1 neurons is indispensable for successful information flow[45] and
266 most probably for performing this computation[46,47] (Fig. 3g). It is tempting to speculate
267 that impaired connectivity of CA1 inputs and resulting impairments in CA1 multimodal
268 input synchrony caused this mis-classification phenotype. The medial EC for example is
269 affected early during the pathology of AD[10,48] and optogenetic stimulation of connections

between dentate gyrus (DG) and EC was sufficient to rescue memory deficits in a mouse model of AD[26]. Furthermore, CA3 input to CA1 neurons might be affected. An impaired dendritic computation of CA1 neurons due to structural and physiological synaptic deficits[49] may also contribute to the observed mis-classification. However, this needs to be further investigated. Our results reveal the neuronal network dysfunction in CA1 as a contributing factor to memory deficits under AD-like conditions and provide relevant evidence that might facilitate the development of a novel strategy to counteract AD-related memory loss.

Acknowledgements

This work was supported by the DZNE, grants from the Deutsche Forschungsgemeinschaft (SFB 1089 C01 and B06), Centres of excellence in Neurodegeneration (CoEN 3018), the ERA-NET MicroSynDep and MicroSchiz project. We thank P. Thevenaz and Erik Meijering for the development of the ImageJ plugins “stackreg” and “TurboReg”. We acknowledge William Wisden for providing the Addgene plasmids #66794 and #66795. We thank Bryan Roth for providing the Addgene plasmid #50475 and the Addgene viral prep #44361. Addgene plasmid #26973 was a gift from Karl Deisseroth. We acknowledge Susanne Schoch and Lioba Dammer for cloning and preparation of viral particles. We thank Simon Wiegert, Stefan Remy, Gabor Petzold, Rafał Czajkowski and Laura Ewell for helpful discussion on the manuscript and the Light Microscope and Animal Facilities of DZNE for constant support.

Author contributions

Conceptualization, M.F. and S.P.; Methodology, S.P. and L.C.J.; Formal Analysis, S.P., M.M., F.M. and J.W.; Investigation, S.P., L.C.J., J.S., M.M. and E.A.G.; Resources, L.D., S.S., B.S., W.S.J. and D.E.; Writing – Original Draft, M.F. and S.P.; Writing – Review & Editing, M.F., S.P., E.A.G.; Visualization, S.P.; Supervision, M.F.; Funding Acquisition, M.F.

Competing interests

The authors declare no competing interests.

References

1 Semon, R. The Mneme. *(G.Allen & Unwin)* (1921).

2 Josselyn, S. a., Köhler, S. & Frankland, P. W. Finding the engram. *Nature Reviews Neuroscience* **16**, 521-534, doi:10.1038/nrn4000 (2015).

3 Guzowski, J. F., McNaughton, B. L., Barnes, C. A. & Worley, P. F. Environment-specific expression of the immediate-early gene Arc in hippocampal neuronal ensembles. *Nat Neurosci* **2**, 1120-1124, doi:10.1038/16046 (1999).

4 Tayler, K. K., Tanaka, K. Z., Reijmers, L. G. & Wiltgen, B. J. Reactivation of neural ensembles during the retrieval of recent and remote memory. *Curr Biol* **23**, 99-106, doi:10.1016/j.cub.2012.11.019 (2013).

5 Reijmers, L. G., Perkins, B. L., Matsuo, N. & Mayford, M. Localization of a Stable Neural Correlate of Associative Memory. *Science* **317**, 1230-1233 (2007).

6 Morgan, J. I., Cohen, D. R., Hempstead, J. L. & Curran, T. Mapping patterns of c-fos expression in the central nervous system after seizure. *Science* **237**, 192-197 (1987).

7 Sagar, S. M., Sharp, F. R. & Curran, T. Expression of c-fos Protein in Brain : Metabolic Mapping at the Cellular Level. *Science* **240**, 5-8 (1988).

8 Schoenenberger, P., Gerosa, D. & Oertner, T. G. Temporal control of immediate early gene induction by light. *PLoS ONE* **4**, e8185, doi:10.1371/journal.pone.0008185 (2009).

9 Fleischmann, A. *et al.* Impaired long-term memory and NR2A-type NMDA receptor-dependent synaptic plasticity in mice lacking c-Fos in the CNS. *J Neurosci* **23**, 9116-9122 (2003).

10 Braak, H. & Braak, E. Neuropathological stageing of Alzheimer-related changes. *Acta Neuropathol* **82**, 239-259 (1991).

11 Prince, M. W., Anders; Guerchet, Maelenn; Ali, Gemma-Claire, Wu, Yu-Tzu; Prina, Matthew. The global impact of dementia - an analysis of prevalence, incidence, cost and trends. (2015).

12 Katzman, R. Editorial: The prevalence and malignancy of Alzheimer disease. A major killer. *Arch Neurol* **33**, 217-218 (1976).

13 Palop, J. J. & Mucke, L. Epilepsy and Cognitive Impairments in Alzheimer Disease. *Arch. Neurol.* **66**, doi:10.1001/archneurol.2009.15.Epilepsy (2010).

14 Kerchner, G. A. *et al.* Hippocampal CA1 apical neuropil atrophy in mild Alzheimer disease visualized with 7-T MRI. *Neurology* **75**, 1381-1387, doi:10.1212/WNL.0b013e3181f736a1 (2010).

15 Goshen, I. *et al.* Dynamics of retrieval strategies for remote memories. *Cell* **147**, 678-689, doi:10.1016/j.cell.2011.09.033 (2011).

16 Larkin, M. C., Lykken, C., Tye, L. D., Wickelgren, J. G. & Frank, L. M. Hippocampal output area CA1 broadcasts a generalized novelty signal during an object-place recognition task. *Hippocampus* **24**, 773-783, doi:10.1002/hipo.22268 (2014).

17 Kumaran, D. & Maguire, E. A. Match mismatch processes underlie human hippocampal responses to associative novelty. *J Neurosci* **27**, 8517-8524, doi:27/32/8517 [pii] 10.1523/JNEUROSCI.1677-07.2007 (2007).

18 Lisman, J. E. & Otmakhova, N. A. Storage, recall, and novelty detection of sequences by the hippocampus: elaborating on the SOCRATIC model to account for normal and aberrant effects of dopamine. *Hippocampus* **11**, 551-568, doi:10.1002/hipo.1071 (2001).

19 Busche, M. A. *et al.* Critical role of soluble amyloid-beta for early hippocampal hyperactivity in a mouse model of Alzheimer's disease. *Proc Natl Acad Sci U S A* **109**, 8740-8745, doi:10.1073/pnas.1206171109 (2012).

20 Busche, M. A. *et al.* Clusters of hyperactive neurons near amyloid plaques in a mouse model of Alzheimer's disease. *Science* **321**, 1686-1689, doi:10.1126/science.1162844 (2008).

21 Attardo, A. *et al.* Long-Term Consolidation of Ensemble Neural Plasticity Patterns in Hippocampal Area CA1. *Cell Rep* **25**, 640-650.e642, doi:10.1016/j.celrep.2018.09.064 (2018).

22 Tanaka, Kazumasa Z. *et al.* Cortical Representations Are Reinstated by the Hippocampus during Memory Retrieval. *Neuron* **84**, 347-354, doi:10.1016/j.neuron.2014.09.037 (2014).

23 Trouche, S. *et al.* Recoding a cocaine-place memory engram to a neutral engram in the hippocampus. *Nat Neurosci* **19**, 564-567, doi:10.1038/nn.4250 (2016).

24 Liu, X. *et al.* Optogenetic stimulation of a hippocampal engram activates fear memory recall. *Nature* **484**, 381-385, doi:10.1038/nature11028 (2012).

25 Ryan, T. J., Roy, D. S., Pignatelli, M., Arons, A. & Toggas, S. M. Engram cells retain memory under retrograde amnesia. *Science* **348**, 1007-1013 (2015).

26 Roy, D. S. *et al.* Memory retrieval by activating engram cells in mouse models of early Alzheimer's disease. *Nature* **531**, 508-512, doi:10.1038/nature17172 (2016).

27 Barth, A. L., Gerkin, R. C. & Dean, K. L. Alteration of neuronal firing properties after in vivo experience in a FosGFP transgenic mouse. *J Neurosci* **24**, 6466-6475, doi:10.1523/JNEUROSCI.4737-03.2004 (2004).

28 Jankowsky, J. L. *et al.* Mutant presenilins specifically elevate the levels of the 42 residue beta-amyloid peptide in vivo: evidence for augmentation of a 42-specific gamma secretase. *Hum Mol Genet* **13**, 159-170, doi:10.1093/hmg/ddh019 (2004).

29 Gu, L. *et al.* Long-term in vivo imaging of dendritic spines in the hippocampus reveals structural plasticity. *J. Neurosci.* **34**, 13948-13953, doi:10.1523/JNEUROSCI.1464-14.2014 (2014).

30 Mahringer, D. *et al.* Expression of c-Fos and Arc in hippocampal region CA1 marks neurons that exhibit learning-related activity changes. Preprint at http://biorxiv.org/content/early/2019/2005/2023/644526.abstract (2019).

31 Palop, J. J. *et al.* Vulnerability of dentate granule cells to disruption of arc expression in human amyloid precursor protein transgenic mice. *J Neurosci* **25**, 9686-9693, doi:10.1523/JNEUROSCI.2829-05.2005 (2005).

32 Rudinskiy, N. *et al.* Orchestrated experience-driven Arc responses are disrupted in a mouse model of Alzheimer's disease. *Nat Neurosci* **15**, 1422-1429, doi:10.1038/nn.3199 (2012).

33 Zhang, P., Hirsch, E. C., Damier, P., Duyckaerts, C. & Javoy-Agid, F. c-fos protein-like immunoreactivity: distribution in the human brain and over-expression in the hippocampus of patients with Alzheimer's disease. *Neuroscience* **46**, 9-21 (1992).

34 Anderson, A. J., Cummings, B. J. & Cotman, C. W. Increased immunoreactivity for Jun- and Fos-related proteins in Alzheimer's disease: association with pathology. *Experimental neurology* **125**, 286-295, doi:10.1006/exnr.1994.1031 (1994).

35 Tanaka, K. Z. *et al.* The hippocampal engram maps experience but not place. *Science* **361**, 392-397, doi:10.1126/science.aat5397 (2018).

36 Mau, W. *et al.* The Same Hippocampal CA1 Population Simultaneously Codes Temporal Information over Multiple Timescales. *Curr Biol* **28**, 1499-1508.e1494, doi:10.1016/j.cub.2018.03.051 (2018).

37 Schmid, L. C. *et al.* Dysfunction of Somatostatin-Positive Interneurons Associated with Memory Deficits in an Alzheimer's Disease Model. *Neuron* **92**, 114-125, doi:10.1016/j.neuron.2016.08.034 (2016).

38 Kilgore, M. *et al.* Inhibitors of class 1 histone deacetylases reverse contextual memory deficits in a mouse model of Alzheimer's disease. *Neuropsychopharmacology* **35**, 870-880, doi:10.1038/npp.2009.197 (2010).

39 Radulovic, J., Kammermeier, J. & Spiess, J. Relationship between Fos Production and Classical Fear Conditioning: Effects of Novelty, Latent Inhibition, and Unconditioned Stimulus Preexposure. *J. Neurosci.* **18**, 7452-7461 (1998).

40 Soltesz, I. & Losonczy, A. CA1 pyramidal cell diversity enabling parallel information processing in the hippocampus. *Nat. Neurosci.* **21**, 484-493, doi:10.1038/s41593-018-0118-0 (2018).

41 Wilson, M. A. & McNaughton, B. L. Dynamics of the hippocampal ensemble code for space. *Science* **261**, 1055-1058, doi:10.1126/science.8351520 (1993).

42 Karlsson, M. P. & Frank, L. M. Network dynamics underlying the formation of sparse, informative representations in the hippocampus. *J Neurosci* **28**, 14271-14281, doi:28/52/14271 [pii] 10.1523/JNEUROSCI.4261-08.2008 (2008).

43 Garner, A. R. *et al.* Generation of a synthetic memory trace. *Science (New York, N.Y.)* **335**, 1513-1516, doi:10.1126/science.1214985 (2012).

44 Girardeau, G., Benchenane, K., Wiener, S. I., Buzsaki, G. & Zugaro, M. B. Selective suppression of hippocampal ripples impairs spatial memory. *Nat Neurosci* **12**, 1222-1223, doi:10.1038/nn.2384 (2009).

45 Bittner, K. C. *et al.* Conjunctive input processing drives feature selectivity in hippocampal CA1 neurons. *Nat Neurosci* **18**, 1133-1142, doi:10.1038/nn.4062 (2015).

46 Basu, J. *et al.* A cortico-hippocampal learning rule shapes inhibitory microcircuit activity to enhance hippocampal information flow. *Neuron* **79**, 1208-1221, doi:10.1016/j.neuron.2013.07.001 (2013).

47 Basu, J. & Siegelbaum, S. A. The Corticohippocampal Circuit, Synaptic Plasticity, and Memory. *Cold Spring Harb Perspect Biol* **7**, doi:10.1101/cshperspect.a021733 (2015).

48 Hsia, A. Y. *et al.* Plaque-independent disruption of neural circuits in Alzheimer's disease mouse models. *Proc Natl Acad Sci U S A* **96**, 3228-3233 (1999).

49 Siskova, Z. *et al.* Dendritic structural degeneration is functionally linked to cellular hyperexcitability in a mouse model of Alzheimer's disease. *Neuron* **84**, 1023-1033, doi:10.1016/j.neuron.2014.10.024 (2014).

Figure titles and legends

Fig. 1 Accessing fosGFP expression *in vivo* revealed two sub-populations of CA1 neurons under healthy and AD-like conditions. **a**, Schematic of hippocampal *in vivo* imaging under healthy (fosGFP) and AD-like conditions (fosGFP-APP/PS1 mice). **b**, Timeline and experimental groups to investigate baseline (BL) and learning- and memory-induced (A-A and A-B) fosGFP expression; cFC, contextual fear conditioning; test, memory recall. **c-e**, Two-photon *in vivo* fosGFP expression (**c**, left) and confocal images (**c**, right) plus quantification (**d,e**) of fosGFP- and GAD67-positive neurons in CA1. In **d** and **e**, data from n=3 fosGFP mice. **f**, Illustration of fosGFP expression changes: neurons that gained (ON), lost (OFF) or kept (CON) their fosGFP expression in a day-to-day interval are color-coded in green, magenta and blue, respectively. **g**,**h**, Color-coded images (left) and quantification (right) of ON, OFF and CON in a day-to-day interval neurons during BL in fosGFP (**g**) and fosGFP-APP/PS1 mice (**h**). **i**, Average percentage of ON, OFF and CON neurons during BL in fosGFP and fosGFP-APP/PS1

mice. **j**, Freezing during memory test in the conditioned context A. **k**, Travelled distance in context A before conditioning, pre-shock. **l**, Freezing in a novel context B. **m**-**p**, Color-coded images (left) and quantification (right) of fosGFP expression changes in fosGFP and fosGFP-APP/PS1 mice trained in context A, and tested either in context A (**m**,**n**) or B (**o**,**p**). **q,** Number of ON cells upon d3-4 during BL and A-A/B. Data in **g**-**i** and **m**-**q** from n=7 fosGFP A-A (G_1), n=6 fosGFP-APP/PS1 A-A (G_2), n=6 fosGFP A-B (G_3) and n=3 fosGFP-APP/PS1 A-B (G_4) mice; BL data (**g**-**i**) comprise measurements from 3745 (G_1), 4195 (G_2), 2983 (G_3) and 2025 (G_4) cells, respectively; data including BL and A-A/B imaging (**m**-**q**) comprise measurements from 4322 (G_1), 5099 (G_2), 3755 (G_3) and 2195 (G_4) cells, respectively; statistics were done over mice; data in **j** and **l** from n=13 fosGFP and n=14 fosGFP-APP/PS1 mice; data in **k** from n=15 fosGFP and n=11 fosGFP-APP/PS1 mice (see also Extended Data Fig. 3a,b); **g**-**i** and **m**-**o**, two-way ANOVA with Holm-Sidak's multiple comparison test; **q**, three-way ANOVA with Holm-Sidak's multiple comparison test; **m**-**p**, d0-1 (reference interval) is compared d1-2, d2-3 and d3-4, statistical significant results are marked by asterisks; **j-l**, two-sided unpaired t-test; $^{n.s.}p < 0.05$; $^{*}p < 0.05$; $^{**}p < 0.01$; $^{***}p < 0.001$; for exact p-values see Supplementary Table 1. Data in **e**,**g**-**q** are presented as mean ± SEM; line plots in **g**,**h** and **m**-**p** represent the means (bold lines), SEM (shadings) and individual mouse values (fine lines) of the consecutively measured data at d0-1, d1-2, d2-3 and d3-4; **e**, **i**-**l**, **q**, each data point depicts the value of an individual mouse. Scale bars, 250 µm (**c**, left), 50 µm (**c**, right and **g**).

Fig. 2 Presence of engram cells independent of memory. a, Scheme visualizing fosGFP expression patterns (randomly named from A to O) during four days, either of the baseline period (BL) or the learning and memory period (A-A/B). (**b**) Relative

frequencies of fosGFP expression patterns during A-A/B, comparing experimental groups G_1, G_2, G_3 and G_4. **c**-**f**, Relative frequencies of fosGFP expression patterns during BL and A-A/B for all experimental groups: G_1 (**c**), G_2 (**d**), G_3 (**e**), G_4 (**f**). **g**,**h**, Scheme and pie chart visualizing the expression fate of neurons that gained (ON, **g**) and those that kept (CON, **h**) fosGFP expression upon contextual fear conditioning (cFC); pie charts depict the average fraction of the respective fosGFP expression patterns in relation to the total number of ON or CON neurons, respectively; fosGFP expression patterns C, L, H, A (**g**) and I, J, E, O (**h**) correspond to those shown in (**a**). **i**, Inter-group comparison of the reactivated fraction of ON and CON neurons; i.e. frequency of pattern C and I divided by all neurons that expressed fosGFP upon cFC (ON and CON). **j**, Relative frequency of engram cells (**j**, pattern C and I) during the baseline (BL) and learning and memory period (A-A/B). Data according to Fig. 1 from n=7 fosGFP A-A (G_1), n=6 fosGFP-APP/PS1 A-A (G_2), n=6 fosGFP A-B (G_3) and n=3 fosGFP-APP/PS1 A-B (G_4) mice; data including BL and A-A/B imaging (**m**-**q**) comprise measurements from 4322 (G_1), 5099 (G_2), 3755 (G_3) and 2195 (G_4) cells, respectively; statistics were done over mice. **i**, two-way ANOVA with Holm-Sidak's multiple comparisons test; **j** three-way ANOVA with Holm-Sidak's multiple comparisons test; $^{n.s.}p<0.05$, $*p<0.05$, $**p<0.01$, for exact p-values see Supplementary Table 1. Data are presented as mean ± SEM; each data point depicts the value of an individual mouse.

Fig. 3 Interference of novelty-like cells with memory engram cells impairs recall. a, Scheme visualizing fosGFP expression patterns during imaging sessions d1-d4 that depict a possible expression history of neurons composing the recall network ($fosGFP^+$ on d4). FosGFP expression patterns are randomly named by letters from A to O (see also Extended Data Fig. 6); BL, baseline period; A-A/A, learning and memory period; RN, recall network; $fosGFP^+$, fosGFP-positive; $fosGFP^-$, fosGFP-negative. **b**, Changes of

the relative frequency (Δf_{d4}) of fosGFP expression patterns among RN neurons visualized by a color code; columns represent experimental groups (G_1, G_2, G_3 and G_4), whereas rows show fosGFP expression patterns corresponding to **a**. **c**,**d**, Inter-group comparisons of the change of the relative frequency (Δf_{d4}) of fosGFP expression patterns C and I (**c**, engram cells) and pattern F (**d**, novelty-like cells) among RN neurons. **e**, Quantification of engram to novelty-like cell ratio. **f**, Weighted Pearson correlation coefficients for pairwise comparisons between the Δf_{d4} values of experimental groups G_1, G_2, G_3, and G_4 of data shown in **b**, visualized by a color code (see Supplementary Table 2 for exact values and statistics). **g**, Scheme of CA1 within the hippocampal circuitry (left). Model visualizing the CA1 recall network (RN) under healthy and under AD-like conditions (right). Data according to Fig. 1 from n=7 G_1, n=6 G_2, n=6 G_3 and n=3 G_4 mice; data comprise measurements from 3467 (G_1), 4377 (G_2), 2549 (G_3) and 1766 (G_4) RN cells, respectively; statistics were done over mice; **c**,**d** two-way ANOVA with Holm-Sidak's multiple comparisons test; **f**, two-sided Pearson correlation with post-hoc t-test with Holm-Bonferroni multiple comparison correction; $^{n.s.}p < 0.05$; *p < 0.05; **p < 0.01; for exact p-values see Supplementary Table 1 and 2. Data are presented as mean ± SEM; each data point depicts the value of an individual mouse.

Fig. 4 Inducing novelty-like activity impaired memory recall whereas reducing it ameliorated memory impairment. a,**b**, Scheme of the experimental setting (**a**) and timeline (**b**) for inducing novelty-like activity (ensemble of neurons active in context B) during memory recall of the conditioned context A. **c**,**d**, Overview (left) and zoom (right) of exemplary confocal images showing CA1 targeted expression of hM3D(Gq)-mCherry in coronal brain slices and stained endogenous c-Fos in vehicle- (**c**) and CNO-treated (**d**) mice; for each mouse, four brain slices were stained and analyzed, with similar results. **e**, Density of c-Fos-positive (c-Fos$^+$) neurons in vehicle- (black) and CNO-treated

(yellow) mice; data from n=7 vehicle-treated and n=8 CNO-treated mice; the value of each mouse represents an average of four analyzed brain slices. **f**, Freezing behavior of vehicle- and CNO-treated mice; data from n=12 vehicle- and n=12 CNO-treated mice. **g**,**h**, Scheme of the experimental setting (**g**) and timeline (**h**) for reducing novelty-like activity (ensemble of neurons active in context B) during memory recall of the conditioned context A. **i**,**j**, Overview (left) and zoom (right) of exemplary confocal images of coronal brain sections showing CA1 targeted expression of hM4D(Gi)-mCherry and MeXO4-stained Aβ plaques; for each mouse, four brain slices were stained and quantified, with similar results; for analysis of hM4D(Gi)-mCherry activation on Fos expression see Extended Data Figure 8. **k**, Freezing behavior of mice, with (**+**) and without (**-**) hM4D(Gi)-tagged neurons. Data in **k** from n=4 APP/PS1(-), n=12 APP/PS1(+), n=4 wild-type(-) and n=13 wild-type (+); **e**,**f**, two-sided unpaired t-test; **k**, two-way ANOVA with Holm-Sidak's multiple comparison test; *p < 0.05; **p < 0.01; ***p < 0.001 for exact p-values see Supplementary Table 1. Data are presented as mean ± SEM; each data point depicts the value of an individual mouse. Scale bars, 500 µm (**c**, left), 25 µm (**c**, right).

Extended Data Fig. 1 *In vivo* fosGFP expression is associated with elevated neuronal activity. a, Scheme of the experimental setting (left) and an exemplary two-photon in *vivo* image showing jRGECO1a and fosGFP expression (right). **b**, Fractions of jRGECO1a-expressing cells that are fosGFP-positive ($fosGFP^+$) or -negative ($fosGFP^-$). **c**, Event frequency of $fosGFP^+$ and $fosGFP^-$ neurons. Data in **b** and **c** from 1953 jRGECO1a-expressing cells in n=4 mice. **d**, Experimental timeline to assess fosGFP expression and its underlying neuronal activity, approximated by the Ca^{2+} event frequency. CE, novel context exposure; CTR, control. **e**-**j**, Exemplary two-photon images (left) and quantification (right) of UP (**e**,**f**), DOWN (**g**,**h**) and no change cells (**i**,**j**). **k**,**l**,

Exemplary two-photon image of jRGECO1a-expressing CA1 neurons (**k**) and respective Ca^{2+} traces (**l**) of identified UP, DOWN and no change neurons marked in **k**. **m**,**n**, Ca^{2+} event frequency of UP, DOWN and no change neurons in the group of mice exposed to a novel context (CE, **m**) and those under continuous anesthesia (CTR, **n**). **o**, Experimental timeline to determine the onset of fosGFP expression upon contextual fear conditioning (cFC). **p**, Exemplary binary two-photon images (left) and quantification (right) of fosGFP expression onset (ON) and decay (OFF). Data in **d**-**n** from n=4 CE and n=6 CTR mice; **c**, two-sided Mann-Whitney test; **f**,**h**,**j**, two-sided unpaired t-test; **m**,**n**, one-way ANOVA with Holm-Sidak's multiple comparison test; $^{n.s}$.p > 0.05; *p < 0.05; **p < 0.01; ***p < 0.001 for exact p-values see Supplementary Table 1. Data in **f**,**h** and **j** are presented as mean ± SEM; each data point depicts the value of an individual mouse. Data in **c m** and **n** show the median (bold line), 25%- and 75%-quartiles (dashed lines), minimum and maximum values (upper and lower end of violins). Scale bars, 50 µm (**a**, right), 5 µm (**e, g, i**), 25 µm (**k**, right).

Extended Data Fig. 2 Characterization of fosGFP expressing neurons. a, Coronal mouse brain section showing the analyzed part (framed) of dorsal CA1. **b**, Quantification of endogenous c-Fos-positive (c-Fos^+) and fosGFP-positive ($fosGFP^+$) neurons in wild-type and fosGFP mice, respectively, and APP/PS1 and fosGFP-APP/PS1 mice; data from n=9 wild-type, n=6 fosGFP, n=5 APP/PS1 and n=9 fosGFP-APP/PS1 mice. **c**, Representative confocal images of c-Fos^+ and $fosGFP^+$ neurons in CA1 of fosGFP and fosGFP-APP/PS1 mice; for each mouse, five brain slices were stained and analyzed (see **d**), with similar results. **d**, Fraction of endogenous c-Fos^+ nuclei that were simultaneously positive for fosGFP; data from n=3 fosGFP and n=3 fosGFP-APP/PS1 mice. **e**-**g**, Method to convert 8-bit raw data into binary images. Exemplary measurement of background fluorescence intensity (BG) in a fosGFP raw data image with manually

placed circular masks (red, ∅ 7.45 μm) (**e**). Exemplary fosGFP raw data (**f**, left) and corresponding binary image (**f**, right). Circular masks (white) were manually placed above putatively fosGFP expressing nuclei to measure their fluorescence intensity (**f**, left). Nuclei with a fosGFP fluorescence intensity above or below threshold (TH) were defined as $fosGFP^+$ or $fosGFP^-$, respectively (**g**). **h**, Images showing the density of $fosGFP^+$ neurons around MeXO4-stained Aß-plaques (yellow) and randomly placed virtual Aß-plaques in fosGFP-APP/PS1 and fosGFP mice, respectively; 250 x 250 μm excerpts of a 1.9 x 1.9 mm field of view; images were acquired once for each mouse; other excerpts show similar results. **i**,**j**, Density of $fosGFP^+$ neurons in CA1 irrespective of Aß plaque distance (**i**), and in the proximity (<50 μm, near) or distant (>50 μm, far) to MeXO4-stained Aß-plaques (**j**) comparing fosGFP-APP/PS1 and fosGFP mice, respectively. **k**, Exemplary images of fosGFP-expressing neurons' fluorescence intensities in CA1 of fosGFP and fosGFP-APP/PS1 mice; 250 x 250 μm excerpts of a 1.9 x 1.9 mm field of view; image was acquired once, other excerpts show similar results; white circles (radius=50 μm) in **h** and **k** depict the area close to a MeXO4-positive Aβ-plaque (in fosGFP-APP/PS1 mice) or a virtual plaque (in fosGFP mice), respectively. **l**,**m**, Fluorescence intensity of fosGFP-expressing neurons in fosGFP and fosGFP-APP/PS1 mice regardless of Aß plaque distance (**l**), and in proximity (<50 μm, near) or distant (>50 μm, far) to MeXO4 stained Aß plaques (**m**); data in **h**-**m** from n=8 fosGFP and n=6 fosGFP-APP/PS1 mice; statistics were done over mice, except for **l** and **m**; data in **l** are from 2873 (fosGFP) and 2092 (fosGFP-APP/PS1) cells; data in **m** are from 1373 (fosGFP – near), 674 (fosGFP-APP/PS1-near), 1500 (fosGFP – far) and 1418 (fosGFP-APP/PS1 – far) cells; **d**,**i**, two-sided unpaired t-test; **j**, two-way ANOVA with Holm-Sidak's correction for multiple comparisons; **l**, two-sided Mann-Whitney test; **m**, Kruskal-Wallis test with Dunn's correction for multiple comparisons; *p <0.05,

631 **p < 0.01, ***p < 0.001, for exact p-values see Supplementary Table 1. Data in **b**,**d**,**i**
632 and **j** are presented as mean ± SEM; each data point depicts the value of an individual
633 mouse. Data in l and m show the median (bold line), 25%- and 75%-quartiles (dashed
634 lines), minimum and maximum values (upper and lower end of violins). Scale bars,
635 40 µm (**c**), 20 µm (**e**,**f**), 50 µm (**h**,**k**).
636
637 **Extended Data Fig. 3 Impaired learning and short-term memory in APP/PS1 mice.**
638 **a**, Experimental protocol for fear conditioning in context A: two minutes of exploration
639 (pre-shock) are followed by three 0.5 mA foot shocks spaced by one minute intervals.
640 Mouse was removed from the chamber one minute after the last foot shock (see also
641 methods section). **b**, Freezing behavior of wild-type and APP/PS1 mice during
642 conditioning. **c**, Experimental paradigm for testing short term memory (STM). **d**,
643 Freezing behavior of wild-type and APP/PS1 mice during STM test, one hour after
644 conditioning. **e**,**f**, Fraction of c-Fos-positive (c-Fos$^+$) per DAPI-positiv (DAPI$^+$) neurons (**e**)
645 and density of DAPI$^+$ neurons upon STM test (**f**). **a**,**b**, Data from n=17 wild-type and n=18
646 APP/PS1 mice; **c**-**f**, data from n=4 wild-type and n=4 APP/PS1 transgenic mice; **b**, two-
647 way ANOVA with Holm-Sidak's correction for multiple comparisons; **d**,**f**, two-sided
648 unpaired t-test; **e**, two-sided Mann-Whitney test; **p < 0.01, for exact p-values see
649 Supplementary Table 1. Data are presented as mean ± SEM; each data point depicts
650 the value of an individual mouse.
651
652 **Extended Data Fig. 4 ON cells upon memory recall.** Inter-group comparison of the
653 fold change of ON cells upon memory recall (d3-4 in A-A/B), corresponding to Fig. 1m-p.
654 Data according to Fig.1, n=7 fosGFP A-A (G_1), n=6 fosGFP-APP/PS1 A-A (G_2), n=6
655 fosGFP A-B (G_3) and n=3 fosGFP-APP/PS1 A-B (G_4) mice; data include BL and A-A/B
656 imaging, comprising measurements from 4322 (G_1), 5099 (G_2), 3755 (G_3) and 2195 (G_4)

cells, respectively; statistics were done over mice; two-way ANOVA with Holm-Sidak's multiple comparisons test; $^{n.s.}p>0.05$, for exact p-values see Supplementary Table 1. Data are presented as mean ± SEM; each data point depicts the value of an individual mouse.

Extended Data Fig. 5 Optogenetic CA1 memory trace activation induces recall in APP/PS1 mice. a, AAV-c-Fos-tTA and AAV-PTRE-tight-hChR2-EYFP were injected bilaterally into the hippocampus of APP/PS1 mice and wild-type littermates (left) before optical fibers were implanted to target CA1 (right). **b**, Experimental timeline. **c**, Representative confocal images showing hChR2-EYFP expression in wild-type (upper) and APP/PS1 mice (lower), respectively; for each mouse, four brain slices were stained and analyzed (see **i**,**j**), with similar results. **d**,**e**, Freezing during the stimulation protocol in context C, before (control, black) and after tagging (hChR2, green) of the same set of APP/PS1 (**d**, left) and wild-type mice (**e**, left). Average freezing during intervals without (off) and with (on) light stimulation in hChR2-tagged APP/PS1 (**d**, right) and wild-type (**e**, right) mice, respectively. **f**,**g**, Freezing during test I (**f**) and test II (**g**) comparing wild-type and APP/PS1 mice. **h**, Comparison of net freezing during light stimulation (on - off, average freezing during light on periods minus average freezing during light off periods) between wild-type and APP/PS1 mice. **i**,**j**, Density of hChR2-positive ($hChR2^+$) cells regardless of Aß plaque distance (**i**), and in proximity (<50 µm, near) or distant (>50 µm, far) to MeXO4 stained Aß plaques in wild-type and APP/PS1 mice (**j**). Data from n=6 wild-type and n=8 APP/PS1 mice; **d** (right), **e** (right), two-sided paired t-test; **f**-**j**, two-sided unpaired t-test; ****p<0.0001, ***p<0.001, for exact p-values see Supplementary Table 1. Data are presented as mean ± SEM; each data point depicts the value of an individual mouse.

683 **Extended Data Fig. 6 Mimicking novelty-like activity in CA1 impaired recall**
684 **performance. a**,**b**, Experimental approach. **c**,**d**, Overview (left) and zoom (right) of
685 exemplary confocal images of coronal brain sections showing CA1 targeted expression
686 of hM3D(Gq)-mCherry and c-Fos in vehicle- (**c**) and CNO-treated mice (**d**); for each
687 mouse, four brain slices were stained and analyzed (see **e**), with similar results. **e**,
688 Density of c-Fos-positive (c-Fos$^+$) neurons in vehicle- and CNO-treated mice; the value
689 of each mouse represents an average of four analyzed brain slices. **f**, Freezing behavior
690 of vehicle- and CNO-treated mice. Data from n=5 CNO-treated and n=4 saline-treated
691 mice; **e**,**f**, two-sided unpaired t-test; ****p<0.0001, *p<0.05, for exact p-values see
692 Supplementary Table 1. Data are presented as mean ± SEM; each data point depicts
693 the value of an individual mouse. Scale bars, 500 µm (**c**, left), 50 µm (**c**, right).
694
695 **Extended Data Fig. 7 Presence of doxycycline prevents DREADD expression. a**,**b**,
696 Experimental approach. **c**, Density of c-Fos-positive (c-Fos$^+$) neurons after memory
697 retrieval; the value of each mouse represents an average of four analyzed brain slices.
698 **d**, Freezing behavior of non-treated and non-labeled mice during recall on d8 (test). **e**,
699 Overview (left) and zoom (right) of an exemplary confocal image of a coronal brain
700 sections showing CA1 lacking expression of hM3D(Gq)-mCherry; for each mouse, four
701 brain slices were stained and analyzed (see **c**), with similar results. Data from n=5 wild-
702 type mice. Data are presented as mean ± SEM; each data point depicts the value of an
703 individual mouse. Scale bars, 500 µm (**e**, left), 50 µm (**e**, right).
704
705 **Extended Data Fig. 8 Reduced endogenous c-Fos expression in hM4D(Gi)-positive**
706 **CA1 pyramidal neurons. a**,**b**, Scheme of the experimental setting (**a**) and timeline (**b**)
707 for reducing noise-like activity (ensemble of neurons active in context B) during memory
708 recall of the conditioned context A (see Fig. 3g-k). **c**,**d**, Intensity distribution of

endogenous c-Fos measured in the nuclei of hM4D(Gi)-mCherry-negative ($mCherry^-$) and hM4D(Gi)-mCherry-positive ($mCherry^+$) cells in both APP/PS1 (**c**) and wild-type mice (**d**). **e**, Quantification of hM4D(Gi)-mCherry expression in wild-type and APP/PS1 mice. Data from n=5 wild-type and n=3 APP/PS1 mice; **c**,**d**, two-sided Mann-Whitney test; **e**, two-sided unpaired t-test; $^{n.s.}p>0.05$; ****p<0.0001, for statistical details and exact p-values see Supplementary Table 1. Data in **c** and **d** show the median (bold line), 25%- and 75%-quartiles (dashed lines), minimum and maximum values (upper and lower end of violins). Data in **e** are presented as mean ± SEM; each data point depicts the value of an individual mouse.

Extended Data Fig. 9 CNO alone has no effect on exploratory behavior or memory recall. a, Travelled distance in context B (left) and freezing in the conditioned context A (right) comparing vehicle- and CNO-treated wild-type mice expressing hM4D(Gi). Data in **a** from n=4 vehicle- and n=8 CNO-treated wild-type mice. **b**, Travelled distances in context B comparing wild-type and APP/PS1 mice expressing hM4D(Gi) (left) or lacking DREADD expression (right); data in **b** (left) from n=8 wild-type and n=10 APP/PS1 mice; data in **b** (right) from n=4 wild-type and n=4 APP/PS1 mice. **c**, Experimental timeline (left). Travelled distance in context B (middle) and freezing in the conditioned context A (right) comparing vehicle- and CNO-treated wild-type mice. Data in **c** from n=6 vehicle-treated and n=7 CNO-treated wild-type mice. **a** (left), two-sided Mann-Whitney test; **a** (right), **b** and **c**, two-sided unpaired t-test; $^{n.s.}p>0.05$, for exact p-values see Supplementary Table 1. Data are presented as mean ± SEM; each data point depicts the value of an individual mouse.

Extended Data Fig. 10 AAV injection and DREADD expression alone have no effect on memory recall. a,**b**, Experimental setup (**a**) and timeline (**b**) to determine the influence of either hM4D(Gi) expression or sham injection (just AAV-c-Fos-tTA) on

memory recall. **c**, Exemplary confocal images showing hM4D(Gi)-mCherry expression in groups A , B and C; for each mouse, four brain slices were stained, with similar results. **d**, Freezing behavior of groups A, B and C during memory test. Data from n=6 group A, n=6 group B and n=6 group C mice. **d**, one-way ANOVA with Holm-Sidaks multiple comparison test; $^{n.s.}p>0.05$, for exact p-values see Supplementary Table 1. Data are presented as mean ± SEM; each data point depicts the value of an individual mouse. Scale bars, 500 µm (**c**, left), 50 µm (**c**, right).

METHODS

Experimental animals

FosGFP and APP_{swe}/PSEN1dE9 (APP/PS1) mice were obtained from The Jackson Laboratory (stock number: 014135) and the Mutant Mouse Regional Resource Center (Stock number: 034832; formerly JAX stock number: 005864), respectively. Both mouse lines were maintained on a C57/BL6 background. FosGFP mice express enhanced green fluorescent protein (EGFP) under the *Fos* promoter resulting in a fosGFP fusion protein. APP/PS1 transgenic mice express human amyloid precursor protein with a Swedish mutation $APP_{K595N/M695L}$ under the mouse prion protein promoter and a mutant human presenilin1 with a deletion of exon 9 (PS1-dE). Heterozygous $fosGFP^{tg/wt}$ and $APP/PS1^{tg/wt}$ were crossbred. $FosGFP^{tg/w}$,$APP/PS1^{wt/wt}$ (fosGFP) and $FosGFP^{tg/w}$,$APP/PS1^{tg/wt}$ (fosGFP-APP/PS1) were selected for experiments, carried out at an age of 13-18 months. Wild-type mice were on a C57/BL6 background and 3-5 month of age. APP/PS1 transgenic mice and wild-type littermates were 14-19 month of age. *Slc17a6*$^{tm2(cre)Lowl}$/J (VGlut2-ires-cre) mice (The Jacksons Laboratory, stock number: 016963) were on a 129S4 background and 6-8 months of age. A summary of the experimental animals used in the manuscript can be found in the Life Sciences Reporting Summary. Mice were group-housed in colonies of up to 5 mice, separated by sex in IVC cages under specific pathogen free (SPF) conditions with unlimited access to food and water. The tap water is preprocessed in three steps to reduce the risk of bacterial and fungal growth: 1. microfiltration, 2. UV decontamination and 3. mild acidification to pH5.5. The light and dark cycle was 12h/12h and the temperature was kept constant at 22°C. Equal numbers of male and female mice were randomly assigned to the experimental groups. Behavioral experiments and imaging was carried out at the light cycle. All procedures were in accordance with an animal protocol approved by the DZNE and the government of North-Rhine-Westphalia.

Hippocampal window surgery

We surgically implanted a unilateral cranial window (∅ 3 mm) on top of the dorsal hippocampus as previously described[29], centered around -1.90 mm (AP) and +2.10 mm (ML) from bregma. The mice were anesthetized with an intraperitoneal injection of ketamine/xylazine (0.13/0.01 mg/g body weight). Additionally, an anti-inflammatory (dexamethasone, 0.2 mg/kg) and an analgesic drug (buprenorphine hydrochloride 0.05 mg/kg; TEMGESIC®, Reckitt Benckiser Healthcare (UK) Ltd., Great Britain) were subcutaneously administered immediately before surgery. The analgesic was applied for three consecutive days after surgery as post-operative treatment. To avoid an experimental bias caused by inflammatory processes, mice were given at least four weeks to completely recover from surgery before *in vivo* imaging started.

Hippocampus two-photon *in vivo* imaging

Fos-driven EGFP expression data were acquired using an upright Zeiss (Carl Zeiss Microscopy GmbH, Jena, Germany) Axio Examiner LSM7MP setup, equipped with a Coherent Cameleon Ultra2 two-photon laser (Coherent, Dieburg, Germany). A 16x water immersion objective with a numerical aperture of 0.8 (Nikon) was used. Enhanced green fluorescent protein (EGFP) was excited at 920 nm. Fluorescence emission was separated by a dichroic mirror (LP555), detecting the green (BP 500-550) and red emitted light (BP 575-610) with non-descanned detectors (NDDs). Image acquisition was performed with ZEN2010 (Carl Zeiss Microscopy GmbH). For each imaging session mice were anesthetized with ketamine/xylazine (0.13/0.01 mg/g body weight). To record fosGFP expression in the dorsal CA1 region of the hippocampus we acquired a tile scan consisting of 3 x 3 separate z-stacks of 120 µm depth with 3 µm z-spacing (0.5 µm/pixels), starting at the surface of the *stratum pyramidale*, thereby spanning a large part of the dorsal CA1 area. For each mouse a similar area of around 0.25 mm^2

795 was analyzed. Repetitive scanning of the same positions over time was achieved by
796 orienting to the vascular pattern under reflected light illumination using a GFP filter set
797 and a metal halide lamp HXP100 (Carl Zeiss Microscopy GmbH, Jena, Germany).
798 Visualization of MeXO4-stained Aβ plaques was achieved by exciting at 780 nm and
799 detecting emission with a BP 450/60 filter. We acquired another 3 x 3 tile scan of 220 µm
800 depth with 5 µm z-spacing during the first imaging session (d0), which was aligned to the
801 fosGFP data in x,y and z, but exceeding it in z, 50 µm below and above. Contextual fear
802 conditioning and memory test were conducted two hours before imaging sessions to
803 ensure induction of fosGFP expression. To avoid handling-evoked fosGFP expression
804 mice were accustomed to the experimenter and to the involved transport between
805 holding and behavior rooms on three consecutive days before the first imaging session.
806 For *in vivo* imaging, mice were anaesthetized and let recover from anesthesia inside
807 their home cage. FosGFP-APP/PS1 transgenic mice received an intraperitoneal dose of
808 50 µg MeXO4 (0,5 µg/µL MeXO4, 10% DMSO, 45% 1,2-Propanediol)[50] during the
809 handling sessions. FosGFP mice received the same volume of the vehicle (solvent
810 without MeXO4). Each mouse underwent ten imaging sessions: five during the baseline
811 period (BL, d0-d4), and five during the learning and memory period (A-A/B, d0-d4),
812 separated by at least two weeks.
813 For the correlation of fosGFP expression with neuronal activity, the *Fos*-driven EGFP
814 signal and jRGECO1a signal were acquired using a galvo-resonant scanner (Thorlabs,
815 Newton, USA) on a custom-built two-photon microscope equipped with a titanium
816 sapphire (Ti:Sa) 80 MHz Cameleon Ultra II two-photon laser (Coherent, Dieburg,
817 Germany). A 16x water immersion objective with a numerical aperture of 0.8 (Nikon) was
818 used. EGFP was excited at 920 nm; the jRGECO1a calcium indicator was excited as
819 980 nm. Fluorescence emission was separated by a dichroic mirror (LP562), detecting
820 the green (BP 525/50) and red emitted light (BP 607/70). The emission signal was

collected using a GaAsP PMT (Thorlabs, Newton, USA). ThorImageLS software (Thorlabs, version 2.1) was used to control image acquisition. 3-5 time series (640 x 343 µm, 0.715 µm/pixel) á 2:50 minutes were acquired at 32.3 Hz.

Correlation of fosGFP expression changes with neuronal activity

Mice were anesthetized using 5% isoflurane, directly after taking them out of their home cage. While being under anesthesia, the mice were head-fixed under the microscope and placed on a custom-built linear treadmill. After the localization of the CA1 pyramidal cell layer, an initial recording of the *Fos*-driven EGFP signal was performed. Then, the anesthesia was removed and the mice were allowed to slowly wake up and experience the treadmill for the first time (CE, context exposure). This moment was defined as minute zero. Recording of jRGECO1a signal was started directly upon removal of anesthesia and performed for the next 15 minutes. Subsequently, another recording of EGFP signal was performed at 60 and 90 minutes. As a control, the same procedure was performed while maintaining a constant anesthesia of 1% isoflurane (CTR, control).

Contextual fear conditioning

The training and the recall for contextual fear conditioning were conducted in a chamber (22 x 20 x 40 cm) composed of transparent plastic walls, a stainless steel grid floor connected to an aversive stimulator/scrambler (Med associates Inc.) and bright light conditions (context A). For training mice were placed in the chamber for 120 seconds before the first foot shock was delivered (0,75 mA, 2 seconds). With an inter-shock interval of 60 seconds two more shocks were applied and mice were returned to the home cage 60 seconds after the third shock. For contextual memory recall mice were placed in the conditioning chamber 2 days after the fear conditioning and were allowed to explore the context for 5 minutes. After every trial the chamber was cleaned by 70%

ethanol. Context B was located in a different room than the conditioning chamber. It was composed of red transparent plastic walls (21 x 21 x 40 cm), a white soft plastic floor and dim light conditions. Here, inter-trial cleaning was conducted with pine flavored 70% ethanol. Context C was composed of white non-transparent MDF (medium density fiber) walls and floor (25 x 25 x 40 cm). For the optogenetic experiment, mice explored context C and context A under fiber-attached conditions and including light stimulation. To assess short-term memory (STM) mice underwent the same training protocol as mentioned above, but were tested 1 hour after conditioning. During training and test mice were video recorded from above by using a camcorder. An experimenter blind to the experimental groups determined the cumulative duration of freezing behavior during the first minute before the first foot shock was applied (pre-shock), and the first 4 minutes of the recall session, manually and offline by using EthoVision XT (Noldus). Freezing was defined as the complete absence of movement, except for breathing.

Adeno-Associated Virus (AAV)

AAV2-DIO-hM3D(Gq)-mCherry (titer: $6.1*10^{12}$ virus genomes/mL) was a gift from Bryan Roth (Addgene viral prep #44361). The plasmids pAAV-c-Fos-tTA-pA (Addgene plasmid #66794) and pAAV-PTRE-tight-hM3D(Gq)-mCherry (Addgene plasmid #66795) were a gift from William Wisden. The plasmids pAAV-PTRE-tight-hM4D(Gi)-mCherry and pAAV-PTRE-tight-hChR2(H134R)-EYFP were prepared by cloning the reading frame of hM4D(Gi)-mCherry and hChR2(H134R)-EYFP obtained from pAAV-hSyn-hM4D(Gi)-mCherry (Addgene plasmid #50475, a gift from Bryan Roth) and pAAV-hSyn-hChR2(H134R)-EYFP (Addgene plasmid #26973, a gift from Karl Deisseroth), respectively into the pAAV-PTRE-tight-hM3D(Gq)-mCherry, thereby replacing the hM3D(Gq)-mCherry. Cloning and preparation of viral particles were conducted by Lioba Dammer (kindly coordinated by Susanne Schoch).

873

874 **AAV injection**

875 For bilaterally injecting AAVs, mice were anesthetized, the hair was removed at the site
876 of incision before wiping it with 70% ethanol. A small incision was made along the
877 midline to expose bregma and the sites of injection by carefully pushing the skin aside.
878 Small holes were drilled and the opening of the dura mater was ascertained. From here
879 the needle was lowered to the depth of interest from brain surface. A volume of 0.5 µl
880 virus per hemisphere was injected with a speed of 0.1 µl/minute. After injecting the virus
881 the needle was left at the site of injection for 10 minutes to allow the virus to diffuse into
882 the tissue. The skin was closed by stitches and mice were given three weeks to recover
883 before experiments started. For targeting CA1 the virus combinations of AAV1/2-c-Fos-
884 tTA with either AAV1/2-PTRE-tight-hChR2(H134R)-EYFP, AAV1/2-PTRE-tight-
885 hM3D(Gq)-mCherry) or AAV1/2-PTRE-tight-hM4(Gi)-mCherry were injected 1:2 at -1.95
886 mm (AP), ± 1.50 mm (ML), -1.15 mm (DV, from brain surface) from bregma. Coordinates
887 for targeting CA1 in VGlut2-ires-cre mice with AAV2-DIO-hM3Dq-mCherry slightly
888 differed to account for the age and background difference of the mice: -1.85 mm (AP), ±
889 1.50 mm (ML), -1.10 mm (DV, from brain surface) from bregma.

890

891

892 **Tagging and manipulating neuronal ensembles**

893 Doxycycline (DOX) was delivered in the preprocessed tap water at 2 mg/ml and
894 5% sucrose from the day of injection[51] in order to prevent tTA-mediated expression. For
895 tagging of neuronal ensembles, mice received preprocessed tap water without DOX for
896 two days before they were exposed to the appropriate context for five minutes. DOX
897 treatment was continued immediately after context exposure. To control for DOX
898 efficiency in preventing the tTA-mediated expression, a group of mice received DOX

899 continuously, while being involved in the same experimental procedures. For activating
900 hM3D(Gq) and hM4D(Gi), 3 µg/g bodyweight CNO (0.4 µg/µl CNO in 0.9% saline,
901 1% DMSO)[52] was injected intraperitoneally, 40 minutes before start of the behavioral
902 task. Control animals received just the solvent (vehicle).
903
904 **Immunohistochemistry**
905 Mice were transcardially perfused with phosphate buffered saline (PBS) pH7.4 followed
906 by 4% paraformaldehyde (PFA) for 5 minutes. Brains were fixed over night in 4% PFA in
907 PBS. Coronal slices of 100 µm thickness were cut on a vibratome (Leica VT 1200, Leica
908 Germany) ranging from -1.60 to -2.60 mm (AP, from bregma). Free-floating slices were
909 permeabilized over night in 0.8% Triton-X100™ and blocked with 4% normal goat serum
910 (ThermoFisher Scientific) plus 4% bovine serum albumin (Carl Roth). To assess fosGFP
911 and endogenous c-Fos expression post-mortem, mice were perfused 120 minutes and
912 90 minutes, respectively, after the behavioral paradigm started. FosGFP fluorescence
913 was enhanced by using an antibody against GFP (chicken anti-GFP 1:1000; ab13970,
914 abcam). Endogenous proto-oncogene c-Fos (c-Fos) was labeled with an antibody
915 against c-Fos (rabbit anti-c-Fos 1:500; sc-52, Santa Cruz Biotechnology). This antibody
916 recognizes the N-terminus of both fosGFP and endogenous c-Fos protein, hence does
917 not allow distinguishing between both. However, neurons that just express endogenous
918 c-Fos can be identified in fosGFP mice if counterstained by a fluorophore different from
919 GFP (see also Extended Data Fig. 2c,d). Inhibitory interneurons were stained with an
920 antibody targeting GAD67 (mouse anti-GAD67 1:1000; MAB5406, Merck Millipore).
921 mCherry fluorescence was enhanced by using an antibody against mCherry (rat anti-
922 mCherry 1:10000; M-11217, ThermoFisher Scientific). Secondary labeling was
923 performed with an Alexa Fluor® 488 goat anti-rabbit (A-11008, ThermoFisher Scientific)
924 and goat anti-chicken (A-11039), and Alexa Fluor® 594 goat anti-rabbit (A-11012,

ThermoFisher Scientific) and goat anti-mouse (R37121), respectively (all 1:400). DAPI was applied 1:5000 during the last 20 minutes of incubation of the secondary antibody. Further details can be found in the Life Sciences Reporting Summary.

Confocal microscopy

Confocal images were acquired using an inverted LSM700 microscope (Carl Zeiss Microscopy GmbH, Jena, Germany) with a 20x air objective. Alexa Fluor® 488 and fosGFP were exited at 488 nm and detected using a 490-555 nm bandpass filter. Alexa Fluor® 594 was excited at 555 nm and detected using a 603-627 nm bandpass filter. MeXO4 and DAPI were excited at 405 nm and detected at a wavelength of 490 nm upwards. The pinhole was set to an airy unit of one. Stacks were acquired with a resolution of 0.62 µm/pixel and a z-spacing of 2 µm.

QUANTIFICATION AND STATISTICAL ANALYSIS

Analysis of two-photon *in vivo* images

Raw data z-stacks were processed with the open source software Fiji (ImageJ 1.46j). Autofluorescence was reduced by subtracting the red from the green channel. Z-stacks spanning the dorsal hippocampal CA1 area (30 slices with 3 µm z-spacing) were maximum intensity projected. Maximum intensity projections of every imaging session were aligned in x-y-dimension using the "TurboReg" plugin[53]. Fluorescence intensities of the background (BG) and of fosGFP-positive ($fosGFP^+$) nuclei were measured within circular masks (∅ 7.45 µm) that were manually placed besides and above potentially $fosGFP^+$ nuclei, respectively. Masks were consecutively numbered, thereby enabling to track and identify fosGFP fluorescence intensity of individual nuclei throughout the experiment. Neurons were categorized as $fosGFP^+$ or $fosGFP^-$ if the signal intensity was above or below threshold (≥ 6 SD above the mean BG fluorescence), respectively.

Obtained binary images were used to calculate the density of fosGFP$^+$ neurons. Density and fosGFP fluorescence intensities near and far from MeXO4-stained Aβ plaques were measured in the data obtained from the first imaging session (BL, d0). To distinguish between fosGFP$^+$ neurons in proximity and distant to a MeXO4-stained Aβ plaques, a circular mask (radius = 50 µm) was centered on the Aβ-plaque, identified in the maximum intensity projection of the respective image. Neurons inside the mask were defined as proximal (<50 µm, near) to the Aβ plaque, neurons outside as distant (>50 µm, far). We randomly applied the masks of fosGFP-APP/PS1 mice to fosGFP mice, to allow for defining fosGFP$^+$ neurons proximal and distant to virtual Aβ plaques in fosGFP mice.

Visualization of fosGFP expression changes

FosGFP expression changes were defined on a day-to-day interval (d0-1, d1-2, d2-3, d3-4). Changes were categorized in ON (from fosGFP$^-$ to fosGFP$^+$), OFF (from fosGFP$^+$ to fosGFP$^-$) and CON (staying fosGFP$^+$). The fractions of ON, OFF and CON neurons were calculated by dividing the total number of neurons in each category by the sum of ON, OFF and CON neurons per day-to-day interval. To calculate the fold change of each category during the learning and memory period (A-A/B), the obtained value was divided by the average baseline value of the corresponding category. Here, d0-1 was used as a reference point for statistical comparisons within genotypes, as no behavioral stimulation preceded. Images containing ON, OFF and CON neurons were generated by pseudo-coloring the circular masks (see also Analysis of two-photon *in vivo* images) with green, magenta and blue, respectively.

fosGFP expression pattern and network similarity analysis

For expression pattern analysis we determined the fosGFP expression on four consecutive days from d1 to d4 during both, the baseline (BL) and learning and memory period (A-A/B). Each neuron can theoretically adopt 1 of 15 different activity pattern (2^4=16, minus 1, for neurons never active) that we randomly named from A to O. We determined the activity pattern of every individual neuron and calculated the relative frequency (f_{rel}) of each pattern relating to the total number of fosGFP$^+$ neurons during the respective imaging period.

For analyzing the activity history of the recall network (RN), i.e. neurons active upon recall, we selected all activity patterns that feature fosGFP expression on d4 (A,B,C,D,F,G,I,O). The relative frequencies f_{d4_BL} and $f_{d4\_A\text{-}A/B}$ of the respective patterns during baseline (BL) and during the learning and memory period (A-A/B, see also Fig. 2a), respectively, were calculated by dividing the number of the observed pattern by the number of neurons fosGFP$^+$ on d4.

To compare the recall network (RN) of the experimental groups, the change of relative frequencies (Δf_{d4}) of any fosGFP expression pattern among the neurons composing the RN was calculated as follows:

$$\Delta f_{d4} = 100 * \frac{f_{d4\_A-A/B} - f_{d4\_BL}}{f_{d4\_BL}},$$

Δf_{d4} is represented by a color code in Fig. 2b. To measure the similarity of recall networks, we correlated the Δf_{d4} values for fosGFP expression patterns A, B, C, D, F, G, I and O of a group with the values of every other group. The correlation coefficient matrix depicts the dimensionless Pearson correlation coefficients, individually weighted by the standard deviation of Δf_{d4} of every pattern[54,55]:

$$w_i = \frac{1}{\left(\frac{\sigma_i}{\sqrt{N_j}^{\lambda}}\right)^{\varkappa}} \qquad \textit{Eq. (1)}$$

where σ_i is the standard deviation of the i-th element in the j-th group with i = A, B, C, D, F, G, I and O and j = 1, 2, 3 and 4. N_j is the size of the j-th group. The exponent $\varkappa$ can be used to differently weight group elements with a high standard deviation. The exponent λ is an additional weighting factor to take into account small group sizes. For instance with $\varkappa=\lambda=1$, the denominator in Eq. (1) gives the default definition of the standard error of the mean (SEM). Due to the large element-by-element and group-by-group variations of the standard deviation and the varying group sizes we use the values $\varkappa=\lambda=4$. Even higher values can be used, but they do not change the results significantly. Eq. (1) is calculated for each element of each group. We conservatively used the largest of the two errors in any pairwise group comparison. The resulting correlation coefficients of every group comparison were summarized in a color-coded matrix (Fig. 2f) and table (Supplementary Table 2). Diagonal entries represent comparisons between identical groups and have the value 1, which represents the highest correlation between two groups. Values from 0 to 1 are depicted by a color code. The range from -1 to 0 is not shown here as our analysis revealed no significant negative correlation coefficients. We computed the corresponding p-values at a 5% significance level for every correlation coefficient[56], including a Holm-Bonferroni correction for multiple comparisons. The exact values of the correlation coefficients and the respective p-values of each pairwise comparison are listed in Supplementary Table 2.

Analysis of confocal images

Nuclei were defined as c-Fos-positive if the measured fluorescence intensities of fosGFP or Alexa Fluor® 488 were above threshold (≥ 6 SD above the mean BG fluorescence).

Analysis of Ca^{2+} event frequency

Motion correction of time-series data was performed using the batch registration function of the custom Fiji macro TurboReg[53]. To measure the fluorescence signal of principal CA1 neurons over time with the aim to determine the Ca^{2+} event frequency, at least five minutes were recorded during epochs when the animal was not running. Regions of interest (ROIs) were drawn manually around individual cell bodies using the open source software ImageJ/Fiji. The change in mean grey value over time was extracted for each ROI and stored as text file.

The ΔF/F was calculated by subtracting the baseline fluorescence F0 from the signal and dividing the value by F0. F0 was defined as the mean of the smallest 20% of all values of a time series. In order to derive an approximation of the neuronal activity from the Ca^{2+} transient frequency, we inferred the underlying spiking activity from the ΔF/F traces. For this, we used the OASIS module for calcium deconvolution[57] that is implemented in the freely available CaImAn toolbox[58]. The algorithm we applied is using the threshold non-negative square (NNLS) method with a deconvolution kernel. The kernel is modeled as the difference between two exponential functions:

$$h(t) = \frac{(e^{-\frac{t}{\tau d}} - e^{-\frac{t}{\tau r}})}{\tau d - \tau r}$$

where τd and τr are the roots of the polynomial, which were chosen to simulate the kinetics of jRGECO1a:

$$f(x) = x^2 - 1.69x + 0.712$$

The algorithm has implemented a constraint on the minimal spike size s_{min} which we set in dependency of the calculated spectral noise (sn)

$$s_{min} = sn * 4$$

The number of inferred spikes was divided by the time of recording to give the frequency.

Identification of UP and DOWN cells

For the correlation of changes in fosGFP expression and neuronal activity, fosGFP expression was determined on three consecutive time points (0 minutes, 60 minutes and 90 minutes). Identification of fosGFP-positive ($fosGFP^+$) cells was performed as described before (see analysis of two-photon *in vivo* images). Cells had to show above-threshold fosGFP expression at one of the three time points in order to be classified as $fosGFP^+$. For all cells that were identified as $fosGFP^+$ cells, the change in fosGFP expression was calculated by subtracting the baseline fosGFP value (at 0 minutes) from the values at the subsequent measurement time points (60 and 90 minutes, respectively).

Cells that at any of the time points showed an increase in either absolute or relative fosGFP expression larger than twice the standard deviation of all changes among the total population of $fosGFP^+$ cells at the respective time point, were classified as UP cells. Cells that showed a decrease larger than the standard deviation were classified as DOWN cells. Cells that did not change their fosGFP intensity above or below these thresholds were classified as "no change" cells. The automatic classification of UP, DOWN and no change cells was furthermore double checked by visual inspection. Note: we suspect the observation of DOWN cells to be independent of stimulus presentation, 90 minutes earlier, as this time interval is shorter than the kinetics of GFP degradation. DOWN cells served as a control for UP cells, as they share the feature of fosGFP transgene expression.

Statistics and Reproducibility

Statistical analysis and preparation of graphs was performed in GraphPad Prism 8 (GraphPad Software Inc., La Jolla, USA). A summary of the study design can be found in the Life Sciences Reporting Summary. We did not apply statistical methods to

predetermine sample sizes, but our chosen sample sizes are similar to those generally employed in the field[26,32]. Subjects were randomly assigned to experimental groups before data acquisition. Assignment was determined by genotype and by aiming at a balanced proportion of sexes in each group. For data collection blinding was not possible. Data analysis was performed blind to the conditions of the experiment via encrypting file names. Mice were excluded from analysis if acquired data sets were incomplete. All data sets were tested for normality with the D'Agostino and Pearson normality test (if n>6) or the Shapiro-Wilk normality test (if n<6). Normally distributed data were tested by using paired and unpaired t-tests, one-way and two-way ANOVAs with Holm-Sidak's multiple comparisons tests. Not normally distributed data were tested by using the Mann-Whitney test or Kruskal-Wallis test with Dunn's correction for multiple comparisons. All statistical test applied in this study were two-sided. For detailed statistics including p-values and confidence intervals see Supplementary Table 1 and 2. Data presentation is described in the legends of the respective Figures.

All animal experiments in this manuscript, but the one in Fig.4g-k, were conducted once, in accordance with the European 3R guideline. The data shown in Fig. 4k, comprising groups APP/PS1 (+) and wild-type (+), were replicated with an independent experiment; pooled results of both experiments are shown. Figures were prepared with Illustrator CS5 Version 15.0.1 (Adobe).

Data Availability

The data that support the findings of this are available from the corresponding author upon request.

Code Availability

The code used for analyzing the data in the current study is available from the corresponding author on request.

Materials & Correspondence

Further information and requests for resources and reagents should be directed to and will be fulfilled by the lead contact, Martin Fuhrmann (martin.fuhrmann@dzne.de).

Methods-only References

50 Burgold, S. *et al.* In vivo multiphoton imaging reveals gradual growth of newborn amyloid plaques over weeks. *Acta Neuropathol* **121**, 327-335, doi:10.1007/s00401-010-0787-6 (2011).

51 Zhu, P. *et al.* Silencing and un-silencing of tetracycline-controlled genes in neurons. *PLoS ONE* **2**, e533, doi:10.1371/journal.pone.0000533 (2007).

52 Lopez, A. J. *et al.* Promoter-Specific Effects of DREADD Modulation on Hippocampal Synaptic Plasticity and Memory Formation. *J Neurosci* **36**, 3588-3599, doi:10.1523/jneurosci.3682-15.2016 (2016).

53 Thevenaz, P., Ruttimann, U. E. & Unser, M. A pyramid approach to subpixel registration based on intensity. *IEEE Trans Image Process* **7**, 27-41, doi:10.1109/83.650848 (1998).

54 Bevington, P. R. & Robinson, D. K. *Data reduction and error analysis for the physical sciences*. 3rd edn, (McGraw-Hill, 2003).

55 Pozzi, F., Di Matteo, T. & Aste, T. Exponential smoothing weighted correlations. *The European Physical Journal B* **85**, 175, doi:10.1140/epjb/e2012-20697-x (2012).

56 Campbell, M. J., Walters, S. J. & Machin, D. *Medical statistics : a textbook for the health sciences*. 4th edn, (Wiley, 2007).

57 Friedrich, J., Zhou, P. & Paninski, L. Fast online deconvolution of calcium imaging data. *PLoS computational biology* **13**, e1005423, doi:10.1371/journal.pcbi.1005423 (2017).

58 Giovannucci, A. *et al.* CaImAn an open source tool for scalable calcium imaging data analysis. *Elife* **8**, doi:10.7554/eLife.38173 (2019).

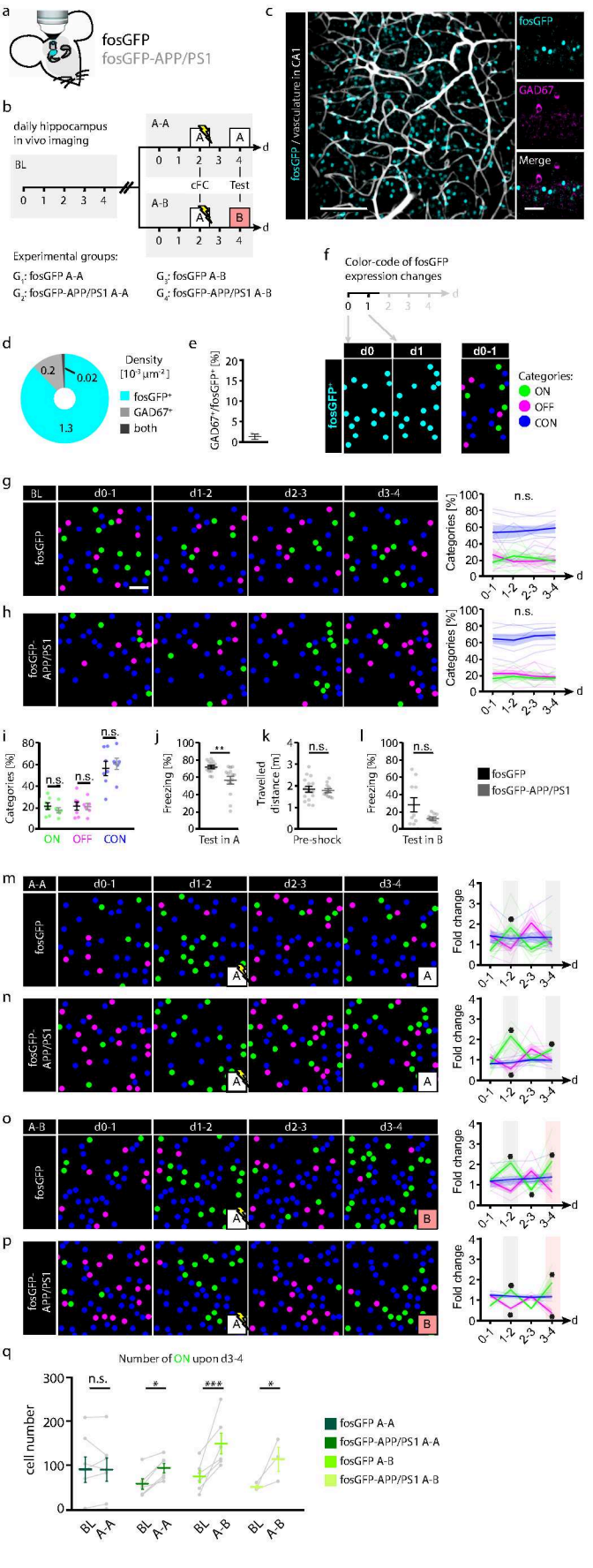
a
fosGFP
fosGFP-APP/PS1
b
daily hippocampus in vivo imaging
BL
A-A
A-B
cFC
Test
d
Experimental groups:
G1: fosGFP A-A
G2: fosGFP-APP/PS1 A-A
G3: fosGFP A-B
G4: fosGFP-APP/PS1 A-B
c
fosGFP / vasculature in CA1
fosGFP
GAD67
Merge
d
Density [10^3 µm^-2]
fosGFP+
GAD67+
both
e
GAD67+/fosGFP+ [%]
f
Color-code of fosGFP expression changes
d0
d1
d0-1
fosGFP+
Categories:
ON
OFF
CON
g
BL
d0-1
d1-2
d2-3
d3-4
fosGFP
Categories [%]
n.s.
h
fosGFP-APP/PS1
i
Categories [%]
n.s.
ON
OFF
CON
j
Freezing [%]
**
Test in A
k
Travelled distance [m]
Pre-shock
l
Freezing [%]
Test in B
fosGFP
fosGFP-APP/PS1
m
A-A
Fold change
n
o
A-B
p
q
Number of ON upon d3-4
cell number
*
***
BL
A-A
A-B
fosGFP A-A
fosGFP-APP/PS1 A-A
fosGFP A-B
fosGFP-APP/PS1 A-B

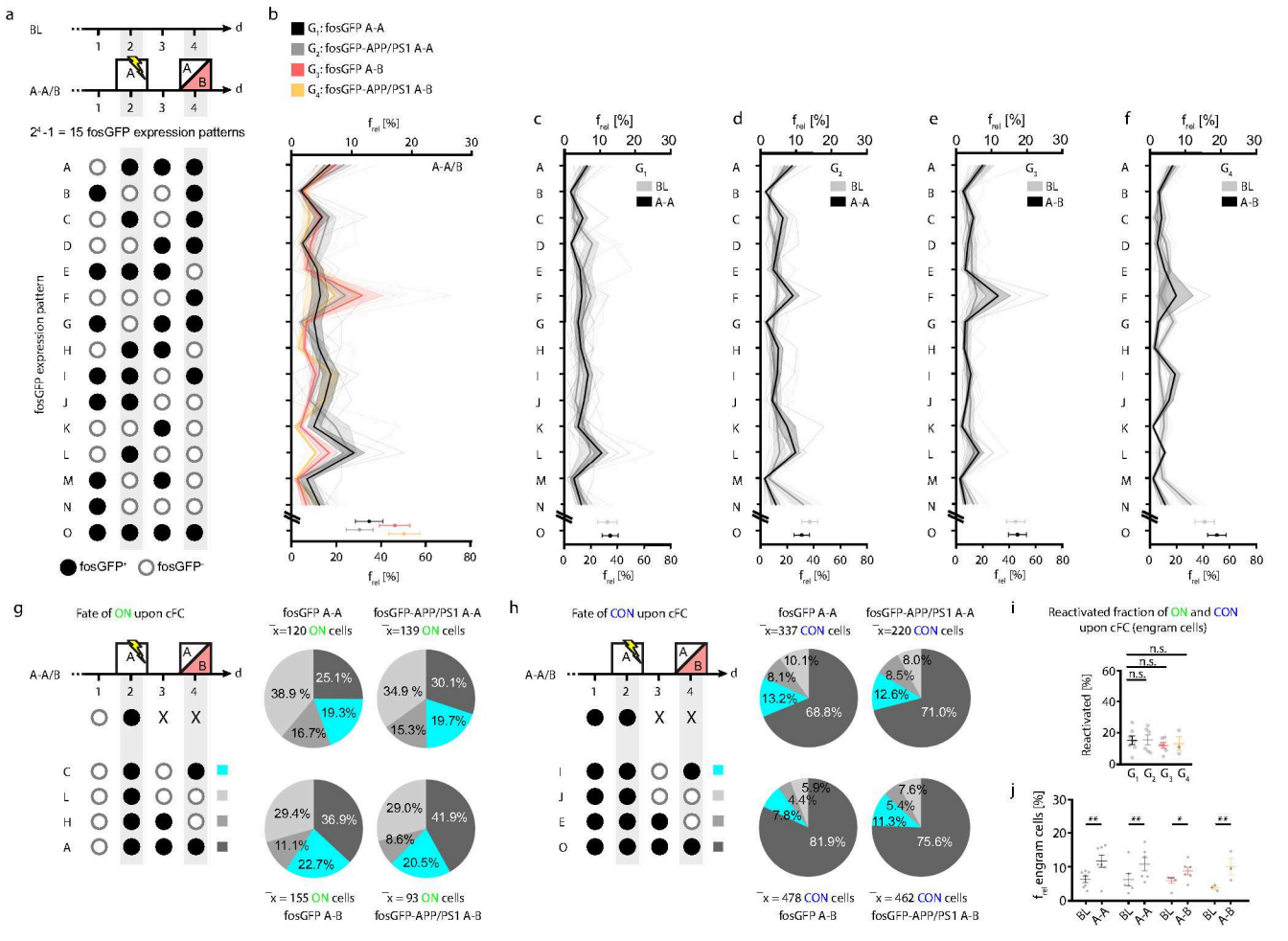
a
BL
A-A/B
d
1 2 3 4
A
A B
2⁴ -1 = 15 fosGFP expression patterns
fosGFP expression pattern
A B C D E F G H I J K L M N O
fosGFP⁺ fosGFP⁻
b
G1: fosGFP A-A
G2: fosGFP-APP/PS1 A-A
G3: fosGFP A-B
G4: fosGFP-APP/PS1 A-B
f_rel [%]
0 10 20 30
A-A/B
0 20 40 60 80
c
d
e
f
G1
G2
G3
G4
BL
A-A
A-B
g
Fate of ON upon cFC
fosGFP A-A
x̄=120 ON cells
fosGFP-APP/PS1 A-A
x̄=139 ON cells
25.1%
19.3%
16.7%
38.9 %
30.1%
19.7%
15.3%
34.9 %
29.4%
36.9%
11.1%
22.7%
29.0%
41.9%
8.6%
20.5%
x̄ = 155 ON cells
fosGFP A-B
x̄ = 93 ON cells
fosGFP-APP/PS1 A-B
h
Fate of CON upon cFC
fosGFP A-A
x̄=337 CON cells
fosGFP-APP/PS1 A-A
x̄=220 CON cells
10.1%
8.1%
13.2%
68.8%
8.0%
8.5%
12.6%
71.0%
5.9%
4.4%
7.8%
81.9%
7.6%
5.4%
11.3%
75.6%
x̄ = 478 CON cells
fosGFP A-B
x̄ = 462 CON cells
fosGFP-APP/PS1 A-B
i
Reactivated fraction of ON and CON upon cFC (engram cells)
Reactivated [%]
n.s.
n.s.
n.s.
0 20 40 60
G1 G2 G3 G4
j
f_rel engram cells [%]
0 10 20 30
**
**
*
**
BL A-A BL A-A BL A-B BL A-B

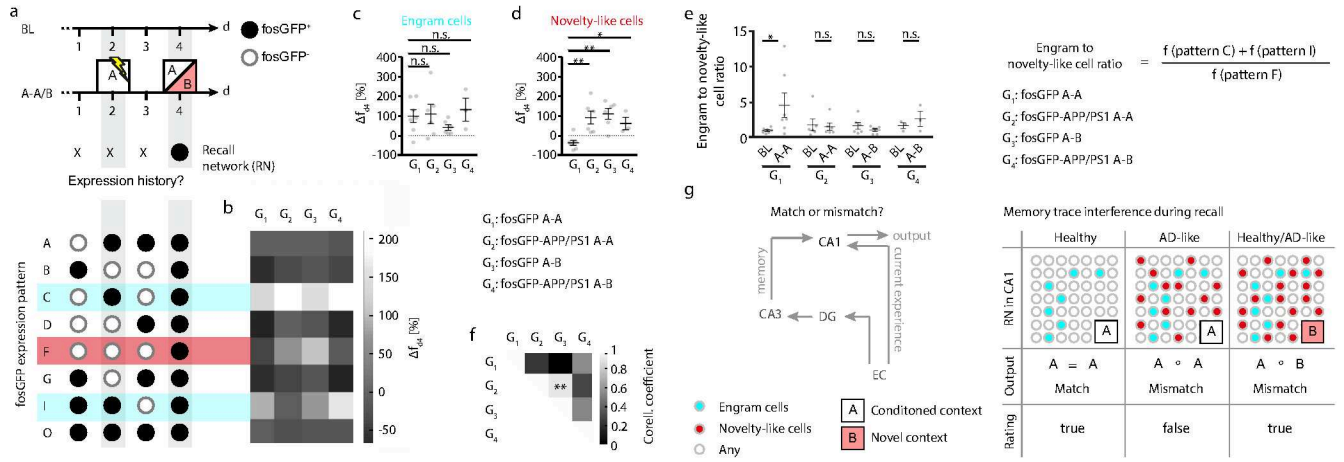
a
BL
A-A/B
d
fosGFP+
fosGFP-
1
2
3
4
A
A
B
X
X
X
Recall
network (RN)
Expression history?
b
G1 G2 G3 G4
fosGFP expression pattern
A
B
C
D
F
G
I
O
200
150
100
50
0
-50
Δf64 [%]
G1: fosGFP A-A
G2: fosGFP-APP/PS1 A-A
G3: fosGFP A-B
G4: fosGFP-APP/PS1 A-B
c
Engram cells
n.s.
n.s.
Δf64 [%]
400
300
200
100
0
-100
G1 G2 G3 G4
d
Novelty-like cells
*
**
**
e
Engram to novelty-like cell ratio
15
10
5
0
*
n.s.
n.s.
n.s.
BL
A-A
A-B
G1
G2
G3
G4
Engram to novelty-like cell ratio = f (pattern C) + f (pattern I) / f (pattern F)
G1: fosGFP A-A
G2: fosGFP-APP/PS1 A-A
G3: fosGFP A-B
G4: fosGFP-APP/PS1 A-B
f
G1 G2 G3 G4
**
1
0.8
0.6
0.4
0.2
0
Corell. coefficient
g
Match or mismatch?
CA1
output
memory
current experience
CA3
DG
EC
Engram cells
Novelty-like cells
Any
A
Conditoned context
B
Novel context
Memory trace interference during recall
Healthy
AD-like
Healthy/AD-like
RN in CA1
A
A
B
Output
A = A
A ∘ A
A ∘ B
Match
Mismatch
Mismatch
Rating
true
false
true

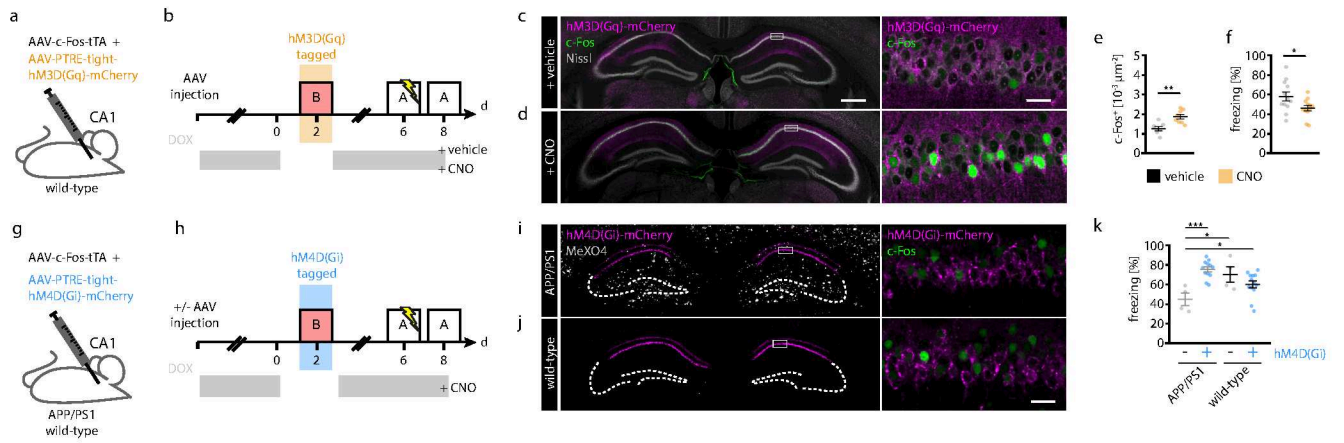
a
AAV-c-Fos-tTA +
AAV-PTRE-tight-
hM3D(Gq)-mCherry
CA1
wild-type
b
hM3D(Gq)
tagged
AAV
injection
B
A
A
d
0
2
6
8
DOX
+ vehicle
+ CNO
c
hM3D(Gq)-mCherry
c-Fos
Nissl
+ vehicle
d
+ CNO
e
c-Fos+ [10-3 µm-2]
**
f
freezing [%]
*
vehicle
CNO
g
AAV-c-Fos-tTA +
AAV-PTRE-tight-
hM4D(Gi)-mCherry
CA1
APP/PS1
wild-type
h
hM4D(Gi)
tagged
+/- AAV
injection
B
A
A
d
0
2
6
8
DOX
+ CNO
i
hM4D(Gi)-mCherry
MeXO4
APP/PS1
j
wild-type
hM4D(Gi)-mCherry
c-Fos
k
freezing [%]
***
*
*
hM4D(Gi)
APP/PS1
wild-type

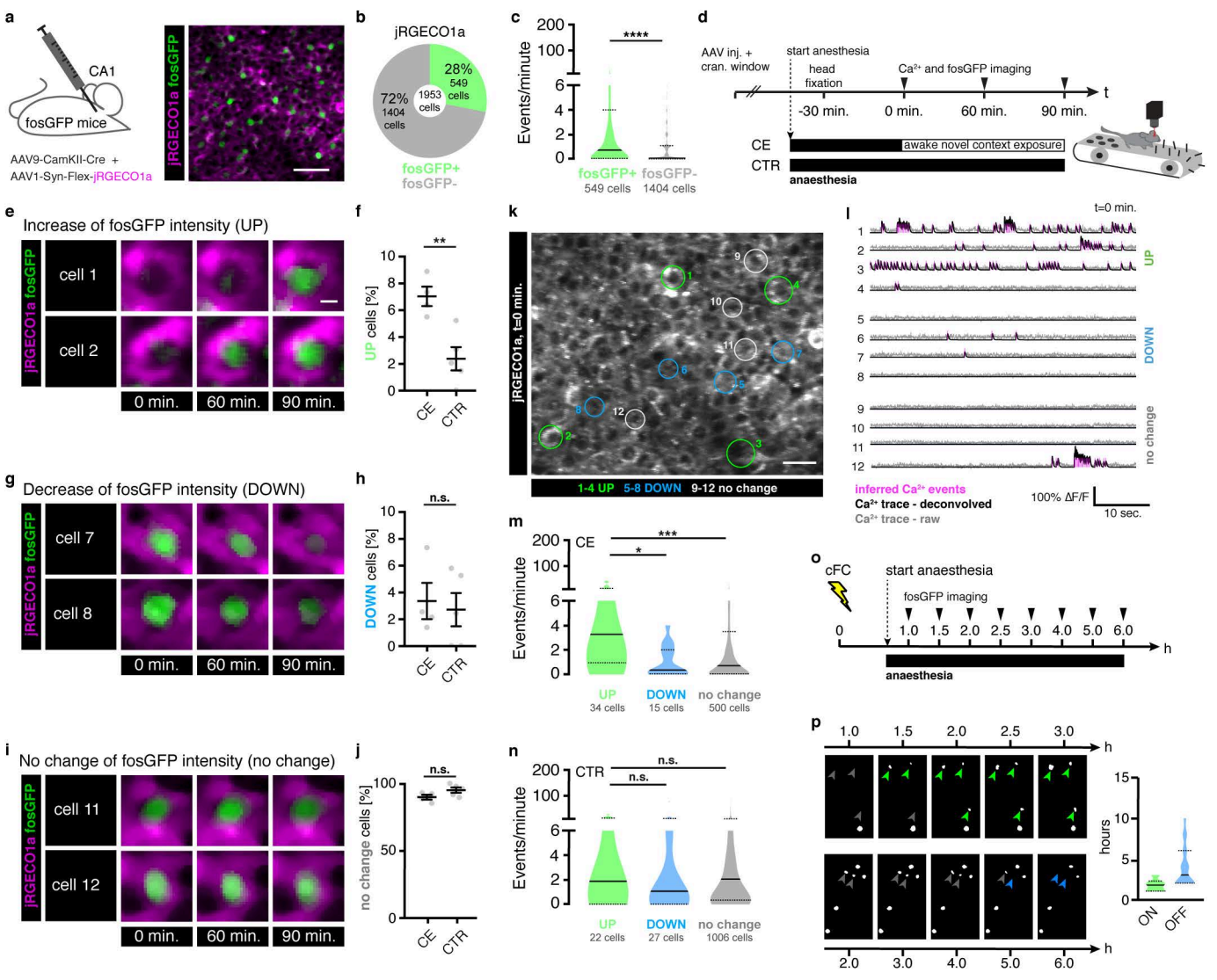
a
CA1
fosGFP mice
AAV9-CamKII-Cre +
AAV1-Syn-Flex-jRGECO1a
jRGECO1a fosGFP
b
jRGECO1a
28%
549 cells
72%
1404 cells
1953 cells
fosGFP+
fosGFP-
c
Events/minute
****
fosGFP+
549 cells
fosGFP-
1404 cells
d
AAV inj. +
cran. window
start anesthesia
head fixation
Ca2+ and fosGFP imaging
t
-30 min.
0 min.
60 min.
90 min.
CE
awake novel context exposure
CTR
anaesthesia
e
Increase of fosGFP intensity (UP)
jRGECO1a fosGFP
cell 1
cell 2
0 min.
60 min.
90 min.
f
UP cells [%]
**
CE
CTR
g
Decrease of fosGFP intensity (DOWN)
jRGECO1a fosGFP
cell 7
cell 8
0 min.
60 min.
90 min.
h
DOWN cells [%]
n.s.
CE
CTR
i
No change of fosGFP intensity (no change)
jRGECO1a fosGFP
cell 11
cell 12
0 min.
60 min.
90 min.
j
no change cells [%]
n.s.
CE
CTR
k
jRGECO1a, t=0 min.
1-4 UP
5-8 DOWN
9-12 no change
l
t=0 min.
UP
DOWN
no change
inferred Ca2+ events
Ca2+ trace - deconvolved
Ca2+ trace - raw
100% ΔF/F
10 sec.
m
CE
Events/minute
***
*
UP
34 cells
DOWN
15 cells
no change
500 cells
n
CTR
Events/minute
n.s.
n.s.
UP
22 cells
DOWN
27 cells
no change
1006 cells
o
cFC
start anaesthesia
fosGFP imaging
0
1.0
1.5
2.0
2.5
3.0
4.0
5.0
6.0
h
anaesthesia
p
1.0
1.5
2.0
2.5
3.0
h
hours
ON
OFF
2.0
3.0
4.0
5.0
6.0
h

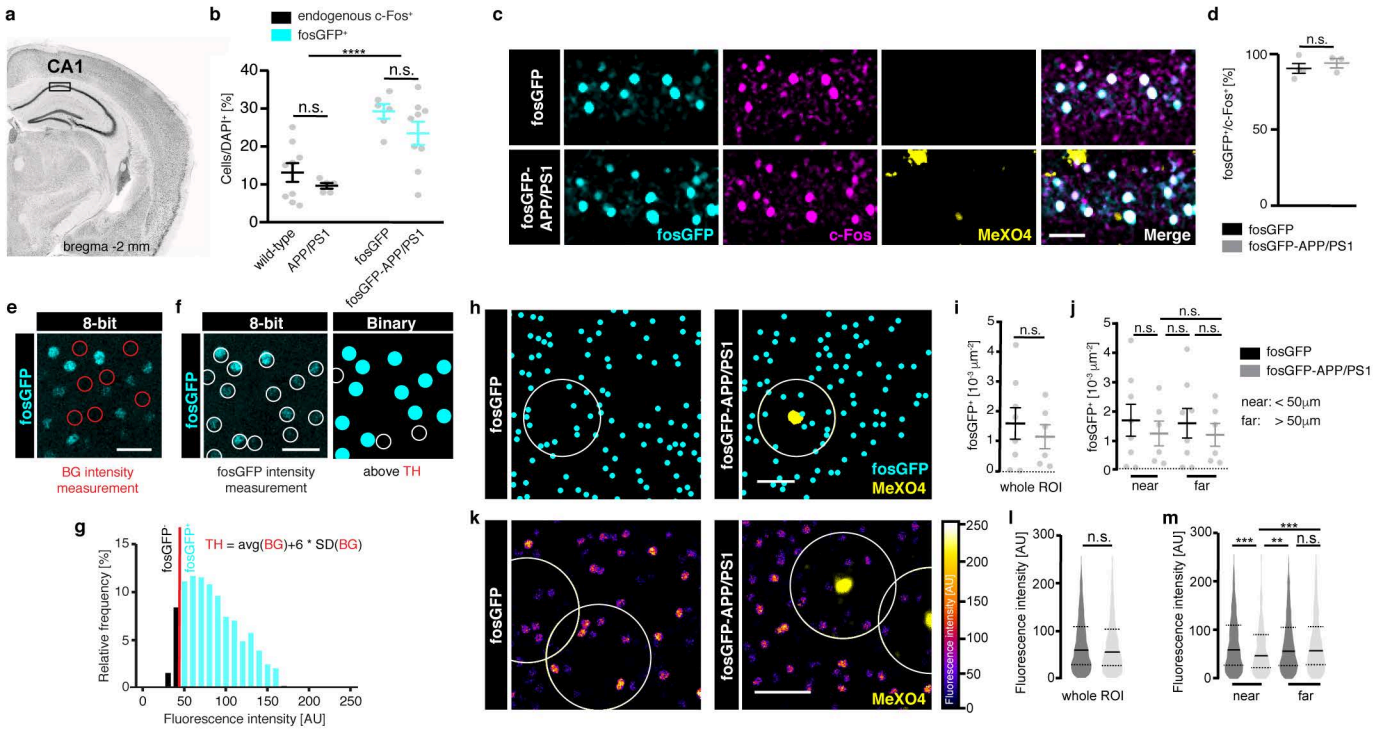
a
CA1
bregma -2 mm
b
endogenous c-Fos+
fosGFP+
Cells/DAPI+ [%]
n.s.
****
n.s.
wild-type
APP/PS1
fosGFP
fosGFP-APP/PS1
c
fosGFP
fosGFP-APP/PS1
fosGFP
c-Fos
MeXO4
Merge
d
n.s.
fosGFP+/c-Fos+ [%]
fosGFP
fosGFP-APP/PS1
e
8-bit
fosGFP
BG intensity measurement
f
8-bit
Binary
fosGFP
fosGFP intensity measurement
above TH
g
fosGFP-
fosGFP+
TH = avg(BG)+6 * SD(BG)
Relative frequency [%]
Fluorescence intensity [AU]
h
fosGFP
fosGFP-APP/PS1
fosGFP
MeXO4
i
n.s.
fosGFP+ [10-3 µm-2]
whole ROI
j
n.s.
n.s.
n.s.
n.s.
fosGFP+ [10-3 µm-2]
near
far
fosGFP
fosGFP-APP/PS1
near: < 50µm
far: > 50µm
k
fosGFP
fosGFP-APP/PS1
MeXO4
Fluorescence intensity [AU]
l
n.s.
Fluorescence intensity [AU]
whole ROI
m
***
**
n.s.
***
Fluorescence intensity [AU]
near
far

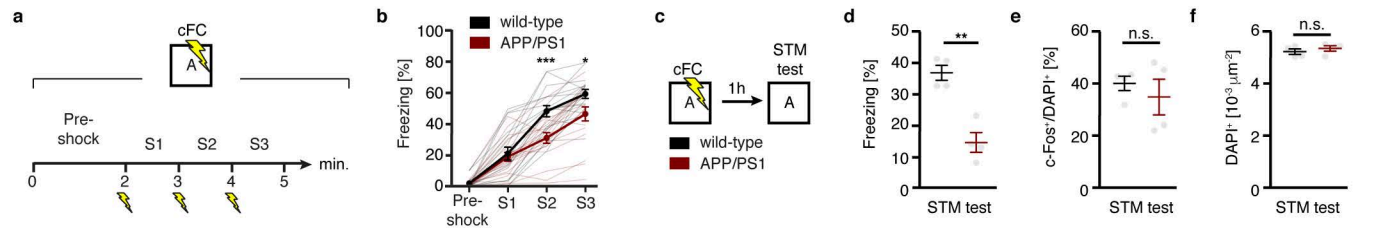
a
cFC
A
Pre-
shock
S1
S2
S3
0
2
3
4
5
min.
b
wild-type
APP/PS1
Freezing [%]
100
80
60
40
20
0
***
*
Pre-
shock
S1
S2
S3
c
cFC
A
1h
STM
test
A
wild-type
APP/PS1
d
Freezing [%]
50
40
30
20
10
0
**
STM test
e
c-Fos+/DAPI+ [%]
60
40
20
0
n.s.
STM test
f
DAPI+ [10-3 µm-2]
6
4
2
0
n.s.
STM test

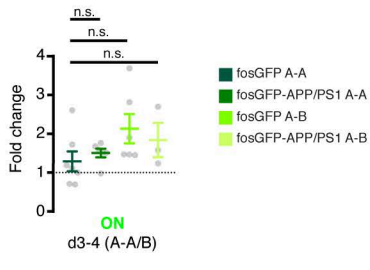
n.s.
n.s.
n.s.
Fold change
4
3
2
1
0
ON
d3-4 (A-A/B)
fosGFP A-A
fosGFP-APP/PS1 A-A
fosGFP A-B
fosGFP-APP/PS1 A-B

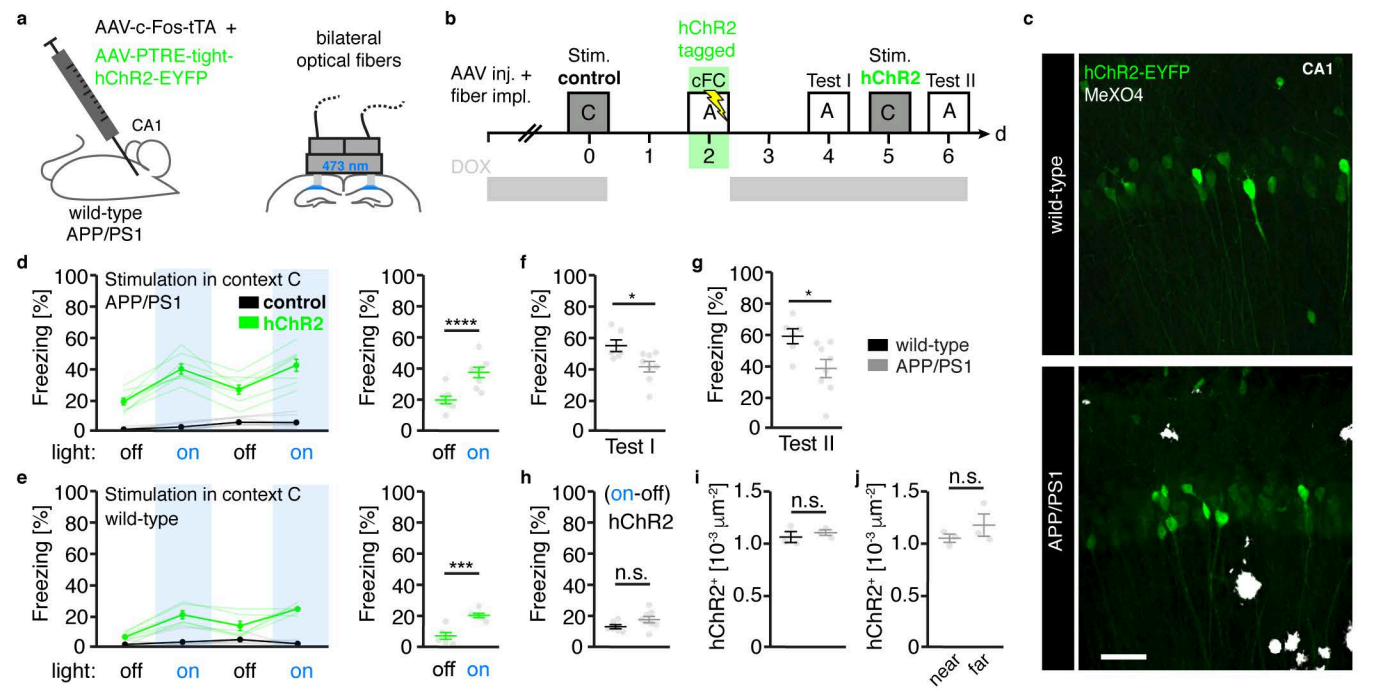
a
AAV-c-Fos-tTA +
AAV-PTRE-tight-
hChR2-EYFP
CA1
wild-type
APP/PS1
bilateral
optical fibers
473 nm
b
AAV inj. +
fiber impl.
Stim.
control
hChR2
tagged
cFC
Test I
Stim.
hChR2
Test II
C
A
A
C
A
DOX
0
1
2
3
4
5
6
d
c
hChR2-EYFP
MeXO4
CA1
wild-type
APP/PS1
d
Stimulation in context C
APP/PS1
control
hChR2
Freezing [%]
light:
off
on
off
on
****
e
Stimulation in context C
wild-type
***
f
*
Test I
g
*
Test II
wild-type
APP/PS1
h
(on-off)
hChR2
n.s.
i
hChR2+ [10-3 µm-2]
n.s.
j
n.s.
near
far

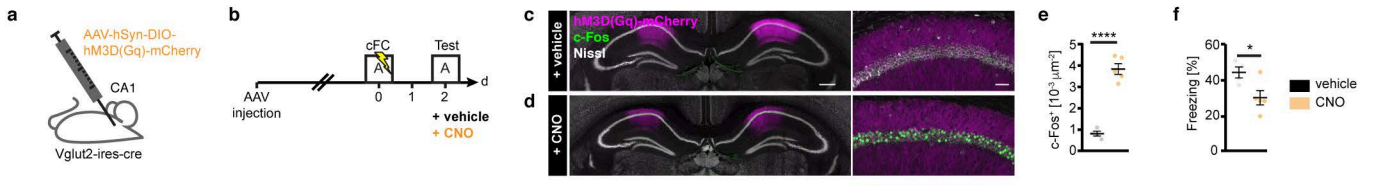
a
AAV-hSyn-DIO-
hM3D(Gq)-mCherry
CA1
Vglut2-ires-cre
b
cFC
Test
A
A
AAV
injection
0
1
2
d
+ vehicle
+ CNO
c
+ vehicle
hM3D(Gq)-mCherry
c-Fos
Nissl
d
+ CNO
e
****
c-Fos+ [10-3 µm-2]
5
4
3
2
1
0
f
*
Freezing [%]
60
40
20
0
vehicle
CNO

a
AAV-c-Fos-tTA +
AAV-PTRE-tight-
hM3D(Gq)-mCherry
CA1
wild-type
b
AAV
injection
B
cFC
Test
A
A
d
0
2
6
8
DOX
non-labeled
non-treated
c
c-Fos+ [10-3 µm-2]
5
4
3
2
1
0
d
Freezing [%]
80
60
40
20
0
e
non-labeled
hM3D(Gq)-mCherry
c-Fos
Nissl

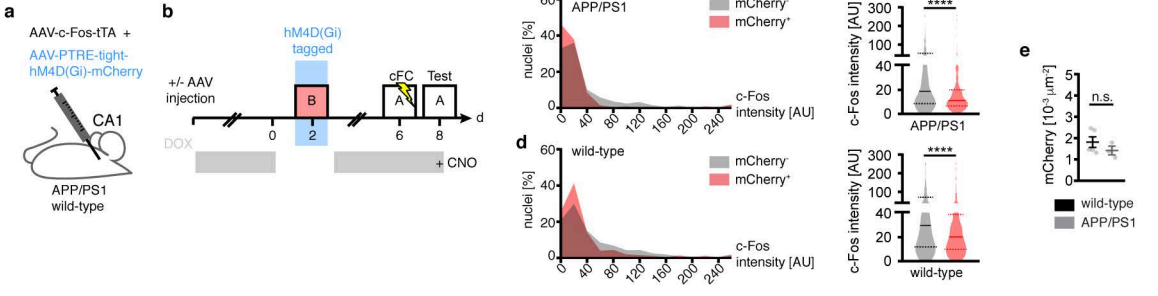
a
AAV-c-Fos-tTA +
AAV-PTRE-tight-hM4D(Gi)-mCherry
CA1
APP/PS1
wild-type
b
hM4D(Gi) tagged
+/- AAV injection
B
cFC
A
Test
A
d
0
2
6
8
DOX
+ CNO
c
APP/PS1
mCherry-
mCherry+
nuclei [%]
c-Fos intensity [AU]
c-Fos intensity [AU]
****
APP/PS1
d
wild-type
mCherry-
mCherry+
nuclei [%]
c-Fos intensity [AU]
c-Fos intensity [AU]
****
wild-type
e
mCherry [10-3 µm-2]
n.s.
wild-type
APP/PS1

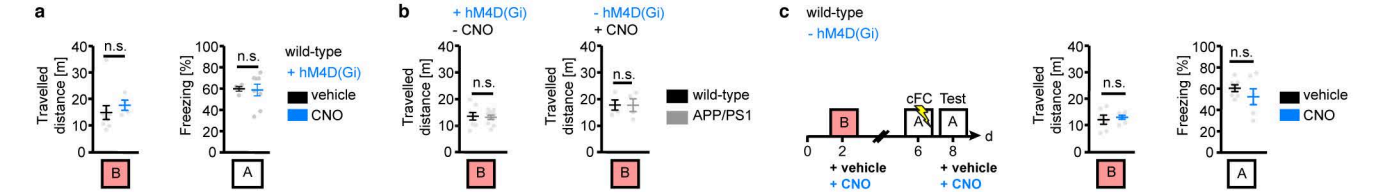
a
Travelled distance [m]
n.s.
B
Freezing [%]
n.s.
A
wild-type
+ hM4D(Gi)
vehicle
CNO
b
+ hM4D(Gi)
- CNO
- hM4D(Gi)
+ CNO
Travelled distance [m]
n.s.
B
wild-type
APP/PS1
c
wild-type
- hM4D(Gi)
cFC
Test
B
A
d
0
2
6
8
+ vehicle
+ CNO
+ vehicle
+ CNO
Travelled distance [m]
n.s.
B
Freezing [%]
n.s.
A
vehicle
CNO

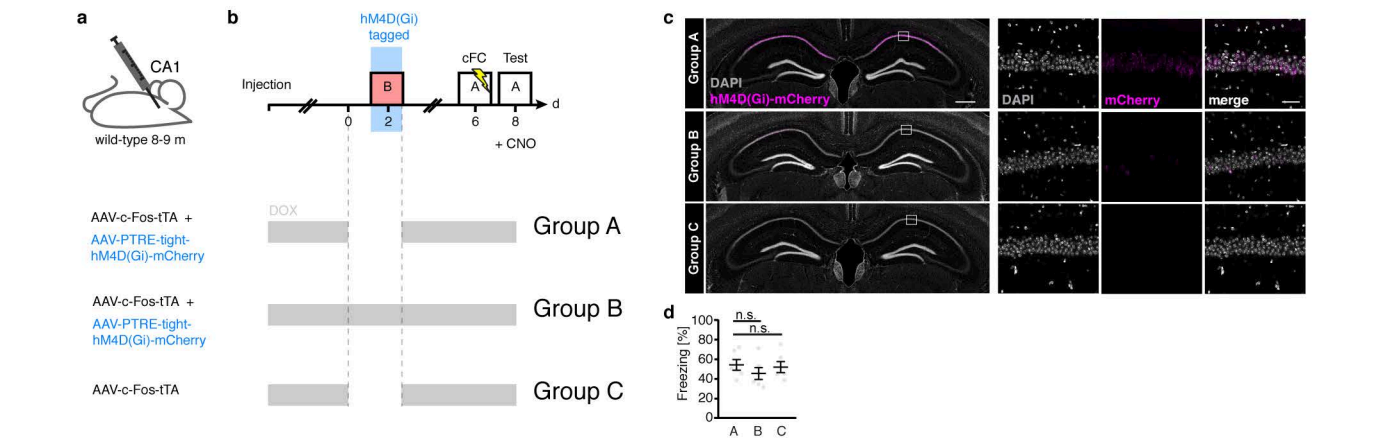
a
CA1
wild-type 8-9 m
b
hM4D(Gi)
tagged
Injection
B
cFC
A
Test
A
d
0
2
6
8
+ CNO
DOX
AAV-c-Fos-tTA +
AAV-PTRE-tight-
hM4D(Gi)-mCherry
Group A
AAV-c-Fos-tTA +
AAV-PTRE-tight-
hM4D(Gi)-mCherry
Group B
AAV-c-Fos-tTA
Group C
c
Group A
Group B
Group C
DAPI
hM4D(Gi)-mCherry
DAPI
mCherry
merge
d
n.s.
n.s.
Freezing [%]
100
80
60
40
20
0
A
B
C

Supplemental information

Memory trace interference impairs recall in a mouse model of Alzheimer's disease

Stefanie Poll[1*], Manuel Mittag[1], Fabrizio Musacchio[1], Lena C. Justus[1], Eleonora Ambrad Giovannetti[1], Julia Steffen[1], Jens Wagner[1], Lioba Dammer[2], Susanne Schoch[2], Boris Schmidt[3], Walker S. Jackson[4], Dan Ehninger[5] and Martin Fuhrmann[1*]

[1]Neuroimmunology and Imaging Group, German Center for Neurodegenerative Diseases (DZNE), Bonn, 53127, Germany.

[2]Institute of Neuropathology, University of Bonn, 53127, Germany

[3]Clemens-Schöpf-Institute, Technical University of Darmstadt, 64289, Germany

[4]Selective Vulnerability of Neurodegenerative Diseases, German Center for Neurodegenerative Diseases (DZNE), Bonn, 53127, Germany

[5]Molecular and Cellular Cognition Group, German Center for Neurodegenerative Diseases (DZNE), Bonn, 53127, Germany

Supplementary Table 1 - Details of statistical tests applied

Notes:

- all statistical tests applied were two-sided
- n was always defined by the number of experimental mice if not stated otherwise
- All data sets were tested for normality with the D'Agostino and Pearson normality test (if n>6) or the Shapiro-Wilk normality test (if n<6)

Figure	Test applied	n		Parameter [unit]	Data presentation	Test results
		exact value	def.			
1g	Two-way repeated measures ANOVA with Holm-Sidak's multiple comparison test	7 fosGFP	Mice	Neuronal categories: ON, OFF and CON [%]	Mean (continuous line) ± SEM (shaded area), fine lines show individual mice	F1, Time: $F(3,54)=0.1.309e-017$, $p>0.9999$ F2, Categories: $F(2,18)=17.88$, $p<0.0001$ F1xF2: $F(6,54)=0.9753$, $p=0.4509$ ON: d0-1 vs. d1-2, $p=0.4789$ ON: d0-1 vs. d2-3, $p=0.6289$ ON: d0-1 vs. d3-4, $p=0.8538$ OFF: d0-1 vs. d1-2, $p=0.4003$ OFF: d0-1 vs. d2-3, $p=0.4003$ OFF: d0-1 vs. d3-4, $p=0.4003$ CON: d0-d1 vs. d1-2, $p=0.9011$ CON: d0-d1 vs. d2-3, $p=0.8667$ CON: d0-d1 vs. d3-4, $p=0.7438$ Lower 95% CI of mean - Upper 95% CI; ON: 9.62 - 27.48 (d0-1), 6.91 - 44.84 (d1-2), 16.10 - 30.69 (d2-3), 10.67 - 28.50 (d3-4) OFF: 9.46 - 45.14 (d0-1), 14.24 - 24.31 (d1-2), 7.75 - 31.85 (d2-3), 6.52 - 35.80 (d3-4) CON: 33.30 - 75.01 (d0-1), 36.75 - 72.96 (d1-2), 44.56 - 69.08 (d2-3), 43.87 - 74.65 (d3-4)
1h	Two-way repeated measures ANOVA with Holm-Sidak's multiple comparison test	6 fosGFP-APP/PS1	Mice	Neuronal categories: ON, OFF and CON [%]	Mean (continuous line) ± SEM (shaded area), fine lines show individual mice	F1, Time: $F(3,45)=0.007067$, $p=0.9992$ F2, Categories: $F(2,15)=45.40$, $p<0.0001$ F1xF2: $F(6,45)=0.8984$, $p=0.5044$ ON: d0-1 vs. d1-2, $p=0.9089$ ON: d0-1 vs. d2-3, $p=0.9897$ ON: d0-1 vs. d3-4, $p=0.9897$ OFF: d0-1 vs. d1-2, $p=0.9684$ OFF: d0-1 vs. d2-3, $p=0.6788$ OFF: d0-1 vs. d3-4, $p=0.6191$ CON: d0-1 vs. d1-2, $p=0.6809$ CON: d0-1 vs. d2-3, $p=0.6409$ CON: d0-1 vs. d3-4, $p=0.6276$ Lower 95% CI of mean - Upper 95% CI; ON: 6.29-28.21 (d0-1), 10.70-28.66 (d1-2), 9.33-26.21 (d2-3), 9.77-25.49 (d3-4) OFF: 15.41-31.10 (d0-1), 13.41-33.42 (d1-2), 5.52-34.62 (d2-3), 9.73-27.88 (d3-4) CON: 48.84 - 80.74 (d0-1), 44.45 - 81.79 (d1-2), 54.53 - 81.89 (d2-3), 56.04 - 82.35 (d3-4)
1i	Two-way ANOVA with Holm-Sidak's multiple comparison test	7 fosGFP 6 fosGFP-APP/PS1	Mice	Average of neuronal categories ON, OFF and CON [%]	Mean ± SEM	F1, Category: $F(2,33)=50.05$, $p<0.0001$ F2, Genotype: $F(1,33)=1.803e-018$, $p>0.999$ F1xF2: $F(2,33)=0.4313$, $p=0.6533$ fosGFP vs. fosGFP-APP/PS1, ON: $p=8696$ OFF: $p=9362$ CON: $p=8696$

						Lower 95% CI of mean - Upper 95% CI; fosGFP: 14.39 - 29.30 (ON), 12.84 - 30.93 (OFF), 40.18 - 72.36 (CON) fosGFP-APP/PS1: 11.93 - 24.24 (ON), 13.77 - 29.00 (OFF), 47.20 - 73.86 (CON)
1j	Two-sided unpaired t-test	13 fosGFP 14 fosGFP-APP/PS1	Mice	Freezing [%]	Mean ± SEM	p=0.0046 t=3.113, df=25 Lower 95% CI of mean - Upper 95% CI; 67.70 - 76.00 (fosGFP), 47.38 - 66.08 (fosGFP-APP/PS1)
1k	Two-sided unpaired t-test	15 fosGFP 11 fosGFP-APP/PS1	Mice	Travelled distance [m]	Mean ± SEM	p=0.7324 t=0.3459, df=24 Lower 95% CI of mean - Upper 95% CI; 1.56 - 2.17 (fosGFP), 1.60 - 2.01 (fosGFP-APP/PS1)
1l	Two-sided unpaired t-test	10 fosGFP 9 fosGFP-APP/PS1	Mice	Freezing [%]	Mean ± SEM	p=0.0933 t=1.1778, df=17 Lower 95% CI of mean - Upper 95% CI; 9.86 - 47.17 (fosGFP), 7.98 - 17.31 (fosGFP-APP/PS1)
1m	Two-way repeated measures ANOVA with Holm-Sidak's multiple comparison test	7 fosGFP A-A (G_1)	Mice	Fold change of neuronal categories: ON, OFF and CON	Mean (continuous line) ± SEM (shaded area), fine lines show individual mice	F1, Time: F(3,54)=0.7248, p=0.5416 F2, Categories: F(2,18)=0.3236, p=0.7277 F1xF2: F(6,54)=7.904, p<0.0001 ON: d0-1 vs. d1-2, p=0.0003 ON: d0-1 vs. d2-3, p=0.8394 ON: d0-1 vs. d3-4, p=0.0701 OFF: d0-1 vs. d1-2, p=0.0603 OFF: d0-1 vs. d2-3, p=0.0603 OFF: d0-1 vs. d3-4, p=0.1098 CON: d0-1 vs. d1-2, p=0.9431 CON: d0-1 vs. d2-3, p=0.9484 CON: d0-1 vs. d3-4, p=0.9484 Lower 95% CI of mean - Upper 95% CI of mean, for ON, OFF and CON. ON: 0.26-1.20 (d0-1), 1.11-2.54 (d1-2), 0.28-1.28 (d2-3), 0.67-1.92 (d3-4) OFF: 0.58-2.29 (d0-1), 0.41-1.21 (d1-2), 1.34-2.77 (d2-3), 0.67-1.34 (d3-4) CON: 0.81-2.10 (d0-1), 0.88-1.71 (d1-2), 0.76-1.94 (d2-3), 0.51-2.20 (d3-4)
1n	Two-way repeated measures ANOVA with Holm-Sidak's multiple comparison test	6 fosGFP-APP/PS1 A-A (G_2)	Mice	Fold change of neuronal categories: ON, OFF and CON	Mean (continuous line) ± SEM (shaded area), fine lines show individual mice	F1, Time: F(3,45)=2.146, p=0.1076 F2, Categories: F(2,15)=7.547, p=0.0054 F1xF2: F(6,45)=9.435, p<0.0001 ON: d0-1 vs. d1-2, p<0.0001 ON: d0-1 vs. d2-3, p=0.2937 ON: d0-1 vs. d3-4, p=0.0054 OFF: d0-1 vs. d1-2, p=0.0452 OFF: d0-1 vs. d2-3, p=0.1563 OFF: d0-1 vs. d3-4, p=0.5204 CON: d0-1 vs. d1-2, p=0.8420 CON: d0-1 vs. d2-3, p=0.7955 CON: d0-1 vs. d3-4, p=0.7955 Lower 95% CI of mean - Upper 95% CI of mean, for ON, OFF and CON. ON: 0.22-1.35 (d0-1), 1.64-2.69 (d1-2), 0.58-1.48 (d2-3), 1.21-1.80 (d3-4) OFF: 0.65-1.62 (d0-1), 0.17-0.95 (d1-2), 0.86-2.22 (d2-3), 0.56-1. 14 (d3-4)

						CON: 0.66-0.98 (d0-1), 0.65-1.08 (d1-2), 0.81-1.20 (d2-3), 0.71-1.26 (d3-4)
1o	Two-way repeated measures ANOVA with Holm-Sidak's multiple comparison test	6 fosGFP A-B (G_3)	Mice	Fold change of neuronal categories: ON, OFF and CON	Mean (continuous line) ± SEM (shaded area), fine lines show individual mice	F1, Time: $F(3,45)=1.196$, $p=0.3222$ F2, Categories: $F(2,15)=2.371$, $p=0.1274$ F1xF2: $F(6,45)=15.49$, $p<0.0001$ ON: d0-1 vs. d1-2, $p=0.0004$ ON: d0-1 vs. d2-3, $p=0.0245$ ON: d0-1 vs. d3-4, $p=0.0002$ OFF: d0-1 vs. d1-2, $p=0.0509$ OFF: d0-1 vs. d2-3, $p=0.0509$ OFF: d0-1 vs. d3-4, $p=0.0509$ CON: d0-1 vs. d1-2, $p=0.7898$ CON: d0-1 vs. d2-3, $p=0.7898$ CON: d0-1 vs. d3-4, $p=0.6879$ Lower 95% CI of mean - Upper 95% CI of mean, for ON, OFF and CON. ON: 0.80-1.66 (d0-1), 1.58-2.55 (d1-2), 0.45-1.06 (d2-3), 1.16-3.11 (d3-4) OFF: 0.66-1.70 (d0-1), 0.35-1.06 (d1-2), 1.07-2.27 (d2-3), 0.42-0.93 (d3-4) CON: 0.72-1.63 (d0-1), 0.80-1.72 (d1-2), 0.86-1.75 (d2-3), 0.79-1.20 (d3-4)
1p	Two-way repeated measures ANOVA with Holm-Sidak's multiple comparison test	3 fosGFP-APP/PS1 (G_4)	Mice	Fold change of neuronal categories: ON, OFF and CON	Mean (continuous line) ± SEM (shaded area), fine lines show individual mice	F1, Time: $F(3,18)=1.196$, $p=0.7051$ F2, Categories: $F(2,6)=9.136$, $p=0.0151$ F1xF2: $F(6,18)=9.398$, $p<0.0001$ ON: d0-1 vs. d1-2, $p=0.0095$ ON: d0-1 vs. d2-3, $p=0.5589$ ON: d0-1 vs. d3-4, $p=0.0006$ OFF: d0-1 vs. d1-2, $p=0.0301$ OFF: d0-1 vs. d2-3, $p=0.8584$ OFF: d0-1 vs. d3-4, $p=0.0062$ CON: d0-1 vs. d1-2, $p=0.9625$ CON: d0-1 vs. d2-3, $p=0.9625$ CON: d0-1 vs. d3-4, $p=0.9625$ Lower 95% CI of mean - Upper 95% CI of mean, for ON, OFF and CON. ON: 0.80-1.66 (d0-1), 1.58-2.55 (d1-2), 0.45-1.06 (d2-3), 1.16-3.11 (d3-4) OFF: 0.66-1.70 (d0-1), 0.35-1.06 (d1-2), 1.07-2.27 (d2-3), 0.42-0.93 (d3-4) CON: 0.79-1.70 (d0-1), 0.92-1.47 (d1-2), 0.83-1.46 (d2-3), 0.65-1.69 (d3-4)
1q	Three-way ANOVA with Holm-Sidak's multiple comparison test	7 fosGFP A-A (G_1) 6 fosGFP-APP/PS1 A-A (G_2) 6 fosGFP A-B (G_3) 3 fosGFP-APP/PS1 A-B (G_4)	Mice	ON cells	Mean ± SEM	F1, Time: $F(1,18)=33.98$, $p<0.0001$ F2, Treatment: $F(1,18)=0.3926$, $p=0.5388$ F3, Genotype: $F(1,18)=0.9842$, $p=0.3343$ F1xF2: $F(1,18)= 11.64$, $p=0.0031$ F1xF3: $F(1,18)=0.6249$, $p=0.4395$ F2xF3: $F(1,18)=0.1152$, $p=0.7382$ F1xF2xF3: $F(1,18)=2.586$, $p=0.1252$ BL vs. A-A/B, G_1: $p=0.9910$ G_2: $p=0.0321$ G_3: $p=0.0001$ G_4: $p=0.0124$ Lower 95% CI of mean - Upper 95% CI of mean, for BL and A-A/B; BL:

						21.97-162.9 (G_1), 29.21-90.97 (G_2), 41.70-111.60 (G_3), 31.49-74.51 (G_4) A-A/B: 27.69-157.5(G_1), 68.3-123.4 (G_2), 91.42-211.6 (G_3), -1.65-233.00 (G_4)
2i	Two-way ANOVA with Holm-Sidak's multiple comparison test	7 fosGFP A-A (G_1) 6 fosGFP-APP/PS1 A-A (G_2) 6 fosGFP A-B (G_3) 3 fosGFP-APP/PS1 A-B (G_4)	Mice	Reactivated [%]	Mean ± SEM	F1, Treatment: $F(1,18)=0.8641$, $p=0.3649$ F2, Genotype: $F(1,18)=0.05191$, $p=0.8223$ F1xF2: $F(1,18)= 0.01584$, $p=0.9012$ G_1 vs. G_2: $p=0.9352$ G_1 vs. G_3: $p=0.7890$ G_1 vs. G_4: $p=0.8795$ Lower 95% CI of mean - Upper 95% CI of mean, for G_1, G_2, G_3 and G_4; 8.49-22.07 (G_1), 7.42-23.78 (G_2), 7.12-16.90 (G_3), -6.10-32.3 (G_4)
2j	Three-way ANOVA with Holm-Sidak's multiple comparison test	7 fosGFP A-A (G_1) 6 fosGFP-APP/PS1 A-A (G_2) 6 fosGFP A-B (G_3) 3 fosGFP-APP/PS1 A-B (G_4)	Mice	f_{rel} engram cells	Mean ± SEM	F1, Time: $F(1,18)= 41.33$, $p<0.0001$ F2, Treatment: $F(1,18)=0.09594$, $p=0.7603$ F3, Genotype: $F(1,18)=1.203$, $p=0.2873$ F1xF2: $F(1,18)= 0.7675$, $p=0.3925$ F1xF3: $F(1,18)=0.06880$, $p=0.7961$ F2xF3: $F(1,18)=0.0006717$, $p=0.9796$ F1xF2xF3: $F(1,18)=1.996$, $p=0.1748$ BL vs. A-A/B (Time), G_1: $p=0.0017$ G_2: $p=0.0097$ G_3: $p=0.0466$ G_4: $p=0.0097$ Lower 95% CI of mean - Upper 95% CI of mean, for BL and A-A/B; BL: 3.95-8.56 (G_1), 1.52-10.79 (G_2), 3.92-7-75 (G_3), 1.50-5.94 (G_4) A-A/B: 7.17-16.10 (G_1), 5.65-15.78 (G_2), 5.75-11.68 (G_3), -0.60-20.67 (G_4)
3c	Two-way ANOVA with Holm-Sidak's multiple comparison test	7 fosGFP A-A (G_1) 6 fosGFP-APP/PS1 A-A (G_2) 6 fosGFP A-B (G_3) 3 fosGFP-APP/PS1 A-B (G_4)	Mice	Relative frequency change, Δf_{d4} [%] of pattern C + I	Mean ± SEM	F1, Treatment: $F(1,18)=0.1969$, $p=0.6625$ F2, Genotype: $F(1,18)=1.589$, $p=0.2235$ F1xF2: $F(1,18)=0.9727$, $p=0.3371$ G_1 vs. G_2: $p=0.8407$ G_1 vs. G_3: $p=0.5992$ G_1 vs. G_4: $p=0.8407$ Lower 95% CI of mean - Upper 95% CI of mean, for G_1, G_2, G_3 and G_4; 19.49-179.10 (G_1), -18.08-138.90 (G_2), 4.71-77.78 (G_3), -121.2-386.10 (G_4)
3d	Two-way ANOVA with Holm-Sidak's multiple comparison test	7 fosGFP A-A (G_1) 6 fosGFP-APP/PS1 A-A (G_2) 6 fosGFP A-B (G_3) 3 fosGFP-APP/PS1 A-B (G_4)	Mice	Relative frequency change, Δf_{d4} [%] of pattern F	Mean ± SEM	F1, Treatment: $F(1,18)=4.525$, $p=0.0475$ F2, Genotype: $F(1,18)=2.047$, $p=0.1697$ F1xF2: $F(1,18)=10.27$, $p=0.0049$ G_1 vs. G_2: $p=0.0029$ G_1 vs. G_3: $p=0.0013$ G_1 vs. G_4: $p=0.0323$ Lower 95% CI of mean - Upper 95% CI of mean, for G_1, G_2, G_3 and G_4; -68.43-(-5.483) (G_1), 6.86-176.90 (G_2), 40.39-182.10 (G_3), -76.08-199.90 (G_4)
3e	Three-way ANOVA with Holm-Sidak's multiple comparison test	7 fosGFP A-A (G_1) 6 fosGFP-APP/PS1 A-A (G_2) 6 fosGFP A-B (G_3) 3 fosGFP-APP/PS1 A-B (G_4)	Mice	Engram-to-novelty-like cell ratio	Mean ± SEM	F1, Time: $F(1,18)= 2.023$, $p=0.1720$ F2, Treatment: $F(1,18)=0.04382$, $p=0.8365$ F3, Genotype: $F(1,18)=0.4103$, $p=0.5299$ F1xF2: $F(1,18)= 0.7903$, $p=0.3857$ F1xF3: $F(1,18)=1.273$, $p=0.2740$ F2xF3: $F(1,18)=1.690$, $p=0.2101$ F1xF2xF3: $F(1,18)=4.291$, $p=0.0530$

						BL vs. A-A/B (Time), G_1: p=0.0166 G_2: p=0.9217 G_3: p=0.9217 G_4: p=0.9217 Lower 95% CI of mean - Upper 95% CI of mean, for BL and A-A/B; BL: 0.61-1.28 (G_1), -0.35-3.88 (G_2), 0.37-2.84 (G_3), -0.11-3.37 (G_4) A-A/B: 0.31-8.70 (G_1), 0.18-2.81 (G_2), 0.50-1.56 (G_3), -2.00-7.17 (G_4)
3f	see Supplementary Table 2					
4e	Two-sided unpaired t-test	7 vehicle-treated 8 CNO-treated	Mice	Fos_+ [10^{-3} μm^{-2}]	Mean ± SEM	p=0.0028 t=3.678, df=13 Lower 95% CI of mean - Upper 95% CI of mean; 1.01-1.56 (vehicle-treated), 1.61-2.17 (CNO-treated)
4f	Two-sided unpaired t-test	12 vehicle-treated 12 CNO-treated	Mice	Freezing [%]	Mean ± SEM	p=0.0379 t=2.209, df=22 Lower 95% CI of mean - Upper 95% CI of mean; 48.44-68.71 (vehicle-treated), 40.38-52.87 (CNO-treated)
4k	Two-way ANOVA with Holm-Sidak's multiple comparison test	4 APP/PS1 (-) 12 APP/PS1 (+) 4 wild-type (-) 13 wild-type (+)	Mice	Freezing [%]	Mean ± SEM	F1, Treatment: F(1,29)=4.504, p=0.0425 F2, Genotype: F(1,29)=1.094, p=0.3042 F1xF2: F(1,29)=17.86, p=0.0001 APP/PS1(-) vs. wild-type(-): p=0.0102 APP/PS1(-) vs. APP/PS1(+): p=0.0003 APP/PS1(-) vs. wild-type(+): p=0.0321 Lower 95% CI of mean - Upper 95% CI of mean; 24.58-65.35 APP/PS1 (-), 69.64-80.99 APP/PS1 (+), 45.02-95.31 wild-type (-), 52.51-67.70 wild-type(+)

Ext. Data Figure	Test applied	n		Parameter [unit]	Data presentation	Test results
		Exact value	def.			
1c	Two-sided Mann-Whitney test	549 fosGFP-positive ($fosGFP_+$) and 1404 fosGFP-negative ($fosGFP_-$) cells	pooled cells of 4 fosGFP mice	Events/ minute	Median, 25%- and 75%-quartiles, borders of plot show minimum and maximum	p<0.0001 Mann Whitney U = 296409 Lower 95% CI of mean - Upper 95% CI of mean; 4.39-6.52 ($fosGFP_+$), 1.49-2.04 ($fosGFP_-$)
1f	Two-sided unpaired t-test	5 CTR 4 CE	Mice	Proportion of UP [%]	Mean ± SEM	p=0.0050 t=4.034, df=7 Lower 95% CI of mean - Upper 95% CI of mean 0.09 4.39 (CTR), 4.22 9.37 (CE)
1h	Two-sided unpaired t-test	5 CTR 4 CE	Mice	Proportion of DOWN [%]	Mean ± SEM	p=0.7358 t=0.3512, df=7 Lower 95% CI of mean - Upper 95% CI of mean; -0.74-6.13 (CTR), -0.96-7.63 (CE)
1j	Two-sided unpaired t-test	5 CTR 4 CE	Mice	Proportion of no change [%]	Mean ± SEM	p=0.0957 t=1.925, df=7 Lower 95% CI of mean - Upper 95% CI of mean; 89.69-100.40 (CTR), 84.15-95.58 (CE)
1m	Kruskal-Wallis test with Dunn's multiple comparison test	34 UP 15 DOWN 500 no change	pooled cells of 4 fosGFP CE mice	Events/ minute	Median, 25%- and 75%-quartiles, borders of plot show minimum and maximum	Kruskal-Wallis statistic 13.42, p=0.0012 UP vs. DOWN: p=0.0189 UP vs. no change: p=0.0007 Lower 95% CI of mean - Upper 95% CI of mean; 4.54-12.48 (UP), 0.35-1.76 (DOWN), 4.24-6.51 (no change)
1n	Kruskal-Wallis test with Dunn's multiple comparison test	22 UP 27 DOWN 1006 no change	pooled cells of 6 fosGFP CTR mice	Events/ minute	see above (1m)	Kruskal-Wallis statistic 1.973, p=0.3728 UP vs. DOWN: p=0.9384 UP vs. no change: p>0.9999 Lower 95% CI of mean - Upper 95% CI of mean; 2.31-9.59 (UP), 0.15-12.16 (DOWN), 8.97-11.61 (no change)
2b	Two-way ANOVA with Holm-Sidak's multiple comparison test	9 wild-type 5 APP/PS1 6 fosGFP 9 fosGFP-APP/PS1	Mice	Neurons/ $DAPI_+$ [%]	Mean ± SEM	F1, Expression: F(1,25)=30.86, p<0.0001 F2, Genotype: F(1,25)=2.988, p=0.0962 F1xF2: F(1,25)=0.1809, p=0.6743 cFos wild-type vs. cFos APP/PS1: p=0.3785 cFos wild-type vs. fosGFP: p=0.0010 cFos wild-type vs. fosGFP-APP/PS1: p=0.0137 cFos APP/PS1 vs. fosGFP: p=0.0006 cFos APP/PS1 vs. fosGFP-APP/PS1: p=0.0066 fosGFP vs. fosGFP-APP/PS1: p=0.2421 Lower 95% CI of mean - Upper 95% CI of mean; 7.54-19.05 (wild-type), 7.65-11.89 (APP/PS1), 24.50-34.46 (fosGFP) 16.61-30.69 (fosGFP-APP/PS1)
2d	Two-sided unpaired t-test	4 fosGFP 3 fosGFP-APP/PS1	Mice	$fosGFP_+$/ $cFos_+$ [%]	Mean ± SEM	p=0.4882 t=0.7478, df=5

						Lower 95% CI of mean - Upper 95% CI of mean; 80.71-101.50 (fosGFP), 81.15-108.10 (fosGFP-APP/PS1)
2i	Two-sided unpaired t-test	8 fosGFP 6 fosGFP-APP/PS1	Mice	$fosGFP_+$ [10^{-3} µm^{-2}]	Mean ± SEM	p=0.5476 t=0.6188, df=12 Lower 95% CI of mean - Upper 95% CI of mean; 0.38-2.87 (fosGFP), 0.14-2.23 (fosGFP-APP/PS1)
2j	Two-way ANOVA with Holm-Sidak's multiple comparison test	8 fosGFP 6 fosGFP-APP/PS1	Mice	$fosGFP_+$ [10^{-3} µm^{-2}]	Mean ± SEM	F1, Distance: F(1,24)=0.02032, p=0.8878 F2, Genotype: F(1,24)=0.7159, p=0.4059 F1xF2: F(1,24)= 0.002741, p=0.9587 fosGFP near vs. fosGFP-APP/PS1 near: p=0.9827 fosGFP far vs. fosGFP-APP/PS1 far p=0.9827 fosGFP far vs. fosGFP-APP/PS1 near p=0.9827 fosGFP-APP/PS1 near vs. fosGFP-APP/PS1 far p=0.9863 Lower 95% CI of mean - Upper 95% CI of mean; 0.37-2.98 (fosGFP - near), 0.12-2.32 (fosGFP-APP/PS1 - near), 0.36-2.79 (fosGFP - far), 0.16-2.19 (fosGFP-APP/PS1 - far)
2l	Two-sided Mann-Whitney test	8 fosGFP 6 fosGFP-APP/PS1	Mice	Intensity [AU]	Median, 25%- and 75%-quartiles, borders of plot show minimum and maximum	p=0.0937 Mann-Whitney U = 2921553 Lower 95% CI of mean - Upper 95% CI of mean; 71.16-75.33 (fosGFP), 69.01-74.05 (fosGFP-APP/PS1)
2m	Kruskal-Wallis test with Dunn's correction for multiple comparisons	8 fosGFP 6 fosGFP-APP/PS1	Mice	Intensity [AU]	see above (2l)	Kruskal-Wallis statistic 19.57, p=0.0002 fosGFP near vs. fosGFP-APP/PS1 near: p=0.0003 fosGFP far vs. fosGFP-APP/PS1 far p>0.9999 fosGFP far vs. fosGFP-APP/PS1 near p=0.0032 fosGFP-APP/PS1 near vs. fosGFP-APP/PS1 far p=0.0004 Lower 95% CI of mean - Upper 95% CI of mean; 71.08-77.12 (fosGFP - near), 60.23-68.68 (fosGFP-APP/PS1 - near), 69.58-75.35 (fosGFP -far), 71.78-78.01 (fosGFP-APP/PS1 - far)
3b	Two-way ANOVA with Holm-Sidak's multiple comparison test	17 wild-type 18 APP/PS1	Mice	Freezing[%]	Mean ± SEM	F1, Time: F(3,99)=185.6, p<0.0001 F2, Genotype: F(1,99)=5.443, p=0.0259 F1xF2: F(3,99)= 6.317, p=0.0006 wild-type vs. APP/PS1, BL: p=0.9868 S1: p=0.8692 S2: p=0.0008 S3: p=0.0142 Lower 95% CI of mean - Upper 95% CI of mean; wild-type: 0.69-4.17 (Pre-Shock), 12.90-30-4 (S1), 41.13-56.48 (S2), 53.76-66.02 (S3) APP/PS1: 1.01-3.66 (Pre-Shock), 13.57-25.51 (S1), 24.34-38.95 (S2), 37.58-56.53 (S3)

3d	Two-sided unpaired t-test	4 wild-type 4 APP/PS1	Mice	Freezing[%]	Mean ± SEM	p=0.0013 t=5.642, df=6 Lower 95% CI of mean - Upper 95% CI of mean; 29.32-44.53 (wild-type), 4.74-24.67 (APP/PS1)
3e	Two-sided Mann-Whitney test	4 wild-type 4 APP/PS1	Mice	cFos$_+$/DAPI$_+$ [%]	Mean ± SEM	p>0.9999 Mann-Whitney U = 8 Lower 95% CI of mean - Upper 95% CI of mean; 31.56-49.01 (wild-type), 13.33-56.80 (APP/PS1)
3f	Two-sided unpaired t-test	4 wild-type 4 APP/PS1	Mice	DAPI$_+$ [10^{-3} µm^{-2}]	Mean ± SEM	p=0.4325 t=0.8411, df=6 Lower 95% CI of mean - Upper 95% CI of mean; 4.88-5.53 (wild-type), 5.00-5.65 (APP/PS1),
4	Two-way ANOVA with Holm-Sidak's multiple comparison test	7 fosGFP A-A (G_1) 6 fosGFP-APP/PS1 A-A (G_2) 6 fosGFP A-B (G_3) 3 fosGFP-APP/PS1 A-B (G_4)	Mice	fold change	Mean ± SEM	F1, Treatment: F(1,18)=3.581, p=0.0747 F2, Genotype: F(1,18)=0.01632, p=0.8998 F1xF2: F(1,18)= 0.67387, p=0.4225 G_1 vs. G_2: p=0.5821 G_1 vs. G_3: p=0.1197 G_1 vs. G_4: p=0.4599 Lower 95% CI of mean - Upper 95% CI of mean for G_1, G_2, G_3 and G_4; *0.67-1.92* (G_1), 1.22-1.80 (G_2), 1.16-3.11 (G_3), -0.06-3.74 (G_4)
5d, right	Two-sided paired t-test	8 APP/PS1	Mice	Freezing[%]	Mean ± SEM	p<0.0001 t=8.793, df=7 Lower 95% CI of mean - Upper 95% CI of mean; 13.98-25.43 (off), 29.54-45.47 (on),
5e, right	Two-sided paired t-test	6 wild-type	Mice	Freezing %]	Mean ± SEM	p=0.0002 t=9.811, df=5 Lower 95% CI of mean - Upper 95% CI of mean; 1.31-12.60 (off), 16.62-23.73 (on)
5f	Two-sided unpaired t-test	6 wild-type 8 APP/PS1	Mice	Freezing[%]	Mean ± SEM	p=0.0223 t=2.622, df=12 Lower 95% CI of mean - Upper 95% CI of mean; 44.82-64.39 (wild-type), 32.90-49.20 (APP/PS1)
5g	Two-sided unpaired t-test	6 wild-type 8 APP/PS1	Mice	Freezing %]	Mean ± SEM	p=0.0226 t=2.614, df=12 Lower 95% CI of mean - Upper 95% CI of mean; 46.44-71.71 (wild-type), 24.07-51.81 (APP/PS1)
5h	Two-sided unpaired t-test	6 wild-type 8 APP/PS1	Mice	Freezing [%]	Mean ± SEM	p=0.1066 t=1.745, df=12 Lower 95% CI of mean - Upper 95% CI of mean; 9.75-16.68 (wild-type), 13.01-22.59 (APP/PS1)
5i	Two-sided	3 wild-type	Mice	hChR2$_+$	Mean ± SEM	p=0.5060

	unpaired t-test	3 APP/PS1		[10^{-3} µm^{-2}]		t=0.7298, df=4 Lower 95% CI of mean - Upper 95% CI of mean; 0.84-1.29 (wild-type), 0.99-1.22 (APP/PS1)
5j	Two-sided unpaired t-test	3 wild-type 3 APP/PS1	Mice	hChR2$_+$ [10^{-3} µm^{-2}]	Mean ± SEM	p=0.3339 t=1.098, df=4 Lower 95% CI of mean - Upper 95% CI of mean; 0.88-1.22 (wild-type), 0.72-1.65 (APP/PS1)
6e	Two-sided unpaired t-test	5 CNO-treated 4 vehicle-treated	Mice	Fos$_+$ [10^{-3} µm^{-2}]	Mean ± SEM	p<0.0001 t=10.06, df=7 Lower 95% CI of mean - Upper 95% CI of mean; 0.43-1.16 (vehicle-treated), 3.12-4.53 (CNO-treated)
6f	Two-sided unpaired t-test	5 CNO-treated 4 vehicle-treated	Mice	Freezing[%]	Mean ± SEM	p=0.0316 t=2.678, df=7 Lower 95% CI of mean - Upper 95% CI of mean; 34.26-54.17 (vehicle-treated), 18.57-41.13 (CNO-treated)
8c, right	Two-sided Mann-Whitney test	1062 mCherry-negative (mCherry$_-$) 201 mCherry-positive (mCherry$_+$)	pooled cells of 3 APP/PS1 mice	Intensity [AU]	Median, 25%- and 75%-quartiles, borders of plot show minimum and maximum	p<0.0001 Mann Whitney U 78979 Lower 95% CI of mean - Upper 95% CI of mean; 38.53-44.84 (mCherry$_-$), 18.06-31.16 (mCherry$_+$),
8d, right	Two-sided Mann-Whitney test	1062 mCherry- negative (mCherry$_-$) 494 mCherry-positive (mCherry$_+$)	pooled cells of 5 wild-type mice	Intensity [AU]	see above (9c, right)	p<0.0001 Mann Whitney U 218609 Lower 95% CI of mean - Upper 95% CI of mean; 47.81-54.67 (mCherry$_-$), 33.16-42.16 (mCherry$_+$)
8e	Two-sided unpaired t-test	5 wild-type 3 APP/PS1	Mice	mCherry$_+$ [10^{-3} µm^{-2}]	Mean ± SEM	p=0.3251 t=1.072, df=6 Lower 95% CI of mean - Upper 95% CI of mean; 1.094-2.48 (wild-type), 0.51-2.28 (APP/PS1)
9a, left	Two-sided Mann-Whitney test	4 vehicle-treated 8 CNO-treated	Mice	Travelled distance [m]	Mean ± SEM	p=0.1483 Mann Whitney U 8 Lower 95% CI of mean - Upper 95% CI of mean; 8.98-1.03 (vehicle-treated), 11.60-23.96 (CNO-treated)
9a, right	Two-sided unpaired t-test	4 vehicle-treated 8 CNO-treated	Mice	Freezing [%]	Mean ± SEM	p=0.8926 t=0.1385, df=10 Lower 95% CI of mean - Upper 95% CI of mean; 52.37-66.25 (vehicle-treated), 45.25-71.14 (CNO-treated)
9b, left	Two-sided unpaired t-test	8 wild-type 10 APP/PS1	Mice	Travelled distance [m]	Mean ± SEM	p=0.8043 t=0.2519, df=16 Lower 95% CI of mean - Upper 95% CI of mean; 11.26-15.02 (wild-type), 10.21-16.86 (APP/PS1)

9b, right	Two-sided unpaired t-test	4 wild-type 4 APP/PS1	Mice	Travelled distance [m]	Mean ± SEM	*p*=0.9871 *t*=0.01682, *df*=6 Lower 95% CI of mean - Upper 95% CI of mean; 11.60-23.96 (wild-type), 10.11-25.35 (APP/PS1)
9c, left	Two-sided unpaired t-test	6 vehicle-treated 7 CNO-treated	Mice	Travelled distance [m]	Mean ± SEM	*p*=0.6253 *t*=0.5023, *df*=11 Lower 95% CI of mean - Upper 95% CI of mean; 7.79-16.59 (vehicle-treated), 11.35-14.78 (CNO-treated)
9c, right	Two-sided unpaired t-test	6 vehicle-treated 7 CNO-treated	Mice	Freezing [%]	Mean ± SEM	*p*=0.3159 *t*=1.051, *df*=11 Lower 95% CI of mean - Upper 95% CI of mean; 52.39-67.66 (vehicle-treated), 33.13-71.01 (CNO-treated)
10d	One-way ANOVA with Holm-Sidak's multiple comparison test	n=6 group A n=6 group B n=6 group C	Mice	Freezing [%]	Mean ± SEM	F1, Treatment: *F*(2,15)=0.6322, *p*=0.5450 A vs. B: *p*=0.5053 A vs. C: *p*=0.7885 Lower 95% CI of mean - Upper 95% CI of mean; 39.95-68.01 (group A), 29.76-60.75 (group B), 37.34-66.22 (group C)

Supplementary Table 2 Correlation coefficients and p-values of the analysis in Figure 2e

a

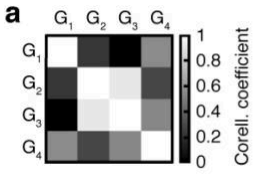

b

	G_1	G_2	G_3	G_4
G_1	1	0.226	-0.076	0.559
G_2	0.226	1	0.919	0.287
G_3	-0.076	0.919	1	0.537
G_4	0.559	0.287	0.537	1

G_1: fosGFP A-A
G_2: fosGFP-APP/PS1 A-A
G_3: fosGFP A-B
G_4: fosGFP-APP/PS1 A-B

c

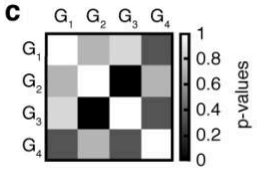

d

	G_1	G_2	G_3	G_4
G_1	1	0.590	0.857	0.150
G_2	0.590	1	0.001	0.491
G_3	0.857	0.001	1	0.170
G_4	0.150	0.491	0.170	1

Recall network of APP/PS1 mice shows high similarity to mice encountering a novel context. a,**b**, Two-sided Pearson correlation coefficients displayed color-coded in a matrix of Fig. 3f (**a**) and numerically in a table (**b**). **c**,**d**, P-values of the correlations in **a** and **b** depicted in a color-code (**c**) and numerically (**d**). Data of Fig. 2, according to Fig. 1 from n=7 fosGFP A-A (G_1), n=6 fosGFP-APP/PS1 A-A (G_2), n=6 fosGFP A-B (G_3) and n=3 fosGFP-APP/PS1 A-B (G_4) mice; data include BL and A-A/B imaging, comprising measurements from 4322 (G_1), 5099 (G_2), 3755 (G_3) and 2195 (G_4) cells, respectively; statistics were done over mice; **a**-**d,** two-sided t-test corrected for multiple comparisons with Holm-Bonferroni.